



HAL
open science

Evidence for major-element heterogeneity in the mantle source of abyssal peridotites from the Southwest Indian Ridge (52° to 68°E)

Monique Seyler, Mathilde Cannat, Catherine Mével

► **To cite this version:**

Monique Seyler, Mathilde Cannat, Catherine Mével. Evidence for major-element heterogeneity in the mantle source of abyssal peridotites from the Southwest Indian Ridge (52° to 68°E). *Geochemistry, Geophysics, Geosystems*, 2003, 4 (2), 10.1029/2002GC000305 . insu-01830158

HAL Id: insu-01830158

<https://insu.hal.science/insu-01830158>

Submitted on 4 Jul 2018

HAL is a multi-disciplinary open access archive for the deposit and dissemination of scientific research documents, whether they are published or not. The documents may come from teaching and research institutions in France or abroad, or from public or private research centers.

L'archive ouverte pluridisciplinaire **HAL**, est destinée au dépôt et à la diffusion de documents scientifiques de niveau recherche, publiés ou non, émanant des établissements d'enseignement et de recherche français ou étrangers, des laboratoires publics ou privés.



Evidence for major-element heterogeneity in the mantle source of abyssal peridotites from the Southwest Indian Ridge (52° to 68°E)

Monique Seyler

*Laboratoire de Géosciences Marines, UMR 7097 - CNRS - Universités Paris 6-7 - Institut de Physique du Globe de Paris, and UFR Sciences de la Terre, Université Lille 1, 59655 Villeneuve d'Ascq cedex, France
(seyler@pop.univ-lille1.fr)*

Mathilde Cannat and Catherine Mével

Laboratoire de Géosciences Marines, UMR 7097 - CNRS - Universités Paris 6-7 - Institut de Physique du Globe de Paris, 4 place Jussieu, 75252, Paris cedex 05, France (cannat@ccr.jussieu.fr; mevel@ccr.jussieu.fr)

[1] A suite of 53 samples of mantle spinel lherzolites and harzburgites dredged at 13 sites between 52°E and 68°E along the Southwest Indian Ridge has been studied for petrography and mineral major element chemistry. Results show that the residual mantle beneath this very slow-spreading/cold ridge is strongly heterogeneous in modal and mineral compositions at local and regional scales and underwent greater extents of melting than predicted by melting model and by compositions of the basalts dredged with the peridotites. Along-axis, the peridotite compositional variability defines a concave pattern with increasing depletion at both ends of the studied section (e.g., approaching Rodrigues Triple Junction to the East and Gallieni fracture zone to the west) that cannot be matched with the basalt compositions. Clinopyroxenes reflect depleted compositions (low modal abundances, high Cr and Mg, low Ti contents) but are paradoxically enriched in jadeite component, a feature that distinguishes these peridotites from common abyssal peridotites. Textural data show that major depletion in basaltic components and pyroxene Na enrichment are early features of the studied peridotites. In most samples, Na is nevertheless correlated with Ti suggesting that initial clinopyroxenes had high Na/Ti contents. Samples at both ends of the studied area have even higher Na/Ti ratios because of higher Na enrichment and higher Ti depletion, indicating metasomatic interaction. We conclude that along-axis compositional variations characterizing these peridotites are primary controlled by major element heterogeneity in the initial mantle, that have been preserved because of low degrees of melting beneath the Southwest Indian Ridge.

Components: 14,397 words, 15 figures, 8 tables.

Keywords: Peridotite; midocean ridge; Indian Ocean; petrology; mantle heterogeneity.

Index Terms: 1025 Geochemistry: Composition of the mantle; 3035 Marine Geology and Geophysics: Midocean ridge processes; 9340 Information Related to Geographic Region: Indian Ocean; 1749 History of Geophysics: Volcanology, geochemistry, and petrology.

Received 14 January 2002; **Revised** 31 July 2002; **Accepted** 2 August 2002; **Published** 6 February 2003.

Seyler, M., M. Cannat, and C. Mével, Evidence for major-element heterogeneity in the mantle source of abyssal peridotites from the Southwest Indian Ridge (52° to 68°E), *Geochem. Geophys. Geosyst.*, 4(2), 9101, doi:10.1029/2002GC000305, 2003.

1. Introduction

[2] This paper is concerned with the petrography and mineral chemistry of mantle peridotites dredged along the axis of the Southwest Indian Ridge in the area comprised between 52°E and 69°E, during the EDUL cruise [Mével, 1997, Figure 1]. Primary mineral compositions and reconstructed bulk compositions are used to infer the degrees of melting, and the source composition of the subaxial mantle in this region of the residual upper mantle.

[3] Decompressional melting beneath mid-oceanic ridges results in the formation of the oceanic crust (melts) and of the lithospheric upper mantle (residues). Whereas mid-oceanic ridge basalt (MORB) compositions integrate the whole melting process and reflect mean extent and mean pressure of melting of the mantle [Klein and Langmuir, 1987; Langmuir *et al.*, 1992], abyssal peridotites of residual composition are expected to reflect the composition of the mantle at the top of the melting column [Dick *et al.*, 1984]. Abyssal peridotite compositions and mineral equilibria may thus provide complementary information on the maximum extent and final pressure of melting in the subaxial mantle.

[4] Beneath ocean ridges, the maximum extent of melting is thought to be a function of the amount of decompression above the solidus, e.g., the melting interval $\Delta P = (P_{\text{initial}} - P_{\text{final}})$. The initial pressure of melting corresponds with the solidus depth, and is controlled by the temperature of the mantle and by its fertility [Dick *et al.*, 1984; McKenzie and Bickle, 1988]. The final pressure of melting is primarily controlled by conductive cooling of the upper mantle beneath the ridge [Bottinga and Allègre, 1978; Reid and Jackson, 1981; Forsyth, 1992; Bown and White, 1994]. If the mantle beneath a ridge is homogeneous in temperature and composition, variations in the extent of melting along this ridge can thus be attributed to variations in the final pressure of melting, reflecting variations in the extent of conductive cooling of the subaxial mantle. Such variations are expected to occur due to ridge segmentation (enhanced cooling of the upper mantle near transform faults [Fox and Gallo, 1984]), or

to variations of spreading rates (enhanced cooling of the upper mantle beneath slow spreading ridges [Bottinga and Allègre, 1978; Reid and Jackson, 1981; Forsyth, 1992; Bown and White, 1994; Shen and Forsyth, 1995]).

[5] The Southwest Indian Ridge (SWIR) is one of the slowest spreading ridges (full rate 1.6 cm/yr [DeMets *et al.*, 1990]) of the global ocean ridge system. The peridotite samples considered in this paper come from the eastern part of the SWIR, between the Gallieni Fracture Zone and the Rodrigues Triple Junction (RTJ; Figure 1). In this region, the ridge axis is anomalously deep (4630 m on average, 4730 m on average between Melville FZ and the RTJ; Figure 2) and high seismic velocities suggest that the underlying mantle is anomalously cold [Debayle and Lévêque, 1997]. Consistent with these features, the crust is inferred to be thinner than average [Francis and Raitt, 1967]. Average crustal thicknesses determined from seismic experiments in this eastern region of the SWIR are indeed smaller than normal (<4.5 km [Muller *et al.*, 1997, 1998; White *et al.*, 2001]), and basalt compositions suggest very low degrees of melting [Dick *et al.*, 1984; Price *et al.*, 1986; Johnson and Dick, 1992; Robinson *et al.*, 1996; Humler *et al.*, 1998; Meyzen *et al.*, 2003].

[6] In this context, we expected our samples to be among the most fertile abyssal peridotites ever reported, and anticipated that very small degrees of melting may have preserved some compositional characteristics (in terms of modal and major element compositions) of the mantle prior to its decompression beneath the ridge. This latter aspect was particularly interesting as Indian Ocean basalts display trace element and isotopic peculiarities that are not yet understood [Dupré and Allègre, 1983; Hart, 1984; Humler *et al.*, 1998; Meyzen *et al.*, 2003].

2. Geological Context and Description of Ultramafic-Bearing Dredges

[7] The area sampled during the EDUL cruise can be subdivided into 2 regions, based on the style of ridge segmentation: the region between Melville FZ and the RTJ is devoid of transform faults

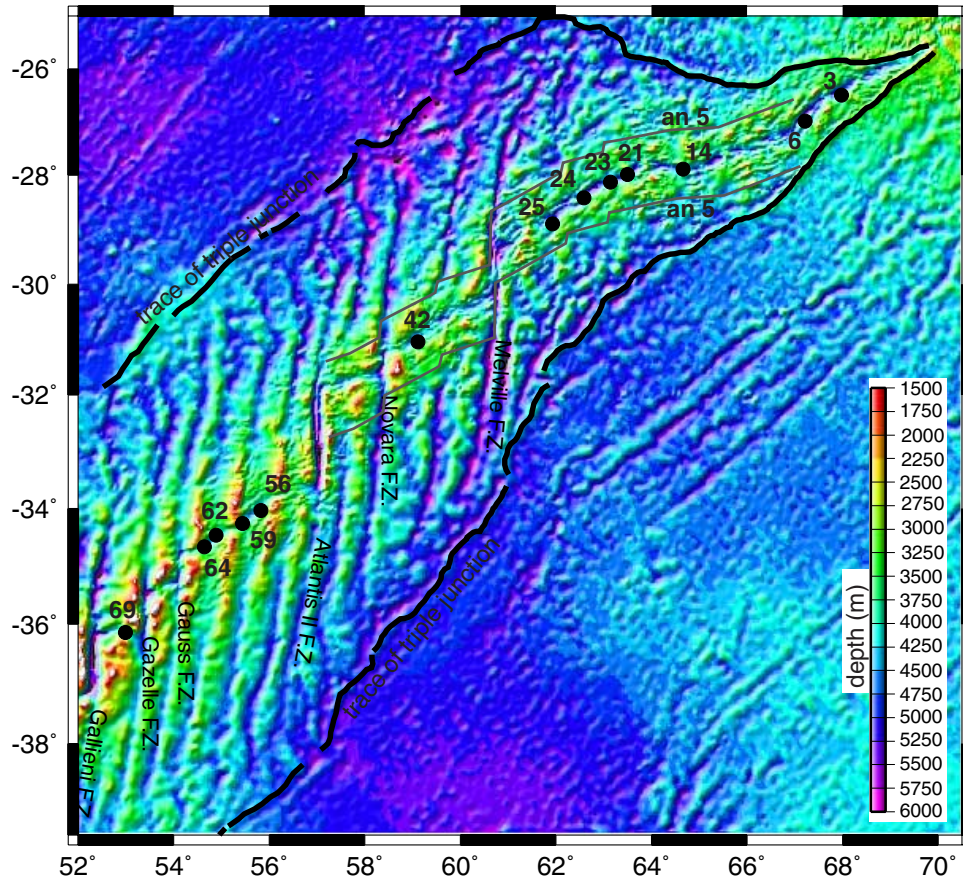


Figure 1. Bathymetric map of the eastern portion of the Southwest Indian Ridge, showing the location of peridotite-bearing dredges from the EDUL cruise. Bathymetry is derived from multichannel shipboard data near the SWIR axis [Mendel et al., 1997], and from satellite altimetry for off-axis areas [Smith and Sandwell, 1994]. Thick lines show the trace of the Rodrigues Triple Junction [Patriat et al., 1997], that separates SWIR crust from Central Indian Ridge and Southeast Indian Ridge crust.

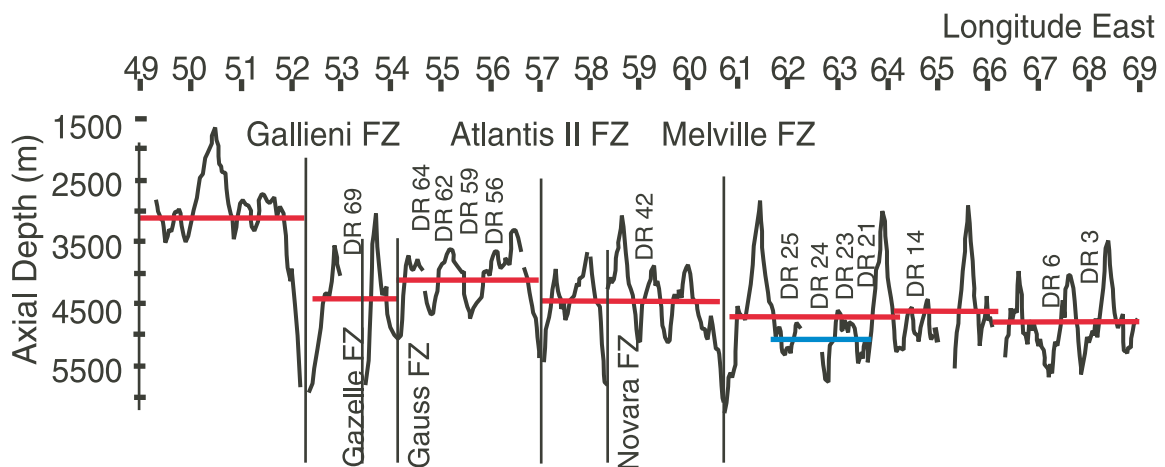


Figure 2. Along axis bathymetry of the SWIR in the study area [after Cannat et al., 1999], showing the location of peridotite-bearing dredges from the EDUL cruise. Lines show the average axial depth in the different portions of the ridge. Average axial depths are greatest in the 62° to 64°E region.

(Figure 1); the region west of Melville FZ comprises five well defined transform faults and five non-transform discontinuities that have persisted through time since the onset of SWIR spreading [Patriat *et al.*, 1997]. Because the SWIR has been propagating eastward at the RTJ, the age of the oldest SWIR crust increases westward from ~ 5 Myr at 69°E , to ~ 64 Myr at 49°E [Patriat and Segoufin, 1988].

[8] The average axial depth is shallower to the west than to the east of Melville FZ (Figure 2), suggesting that average crustal thicknesses and/or mantle temperatures increase toward the west of our study area. A simple model of mantle melting and regional isostatic compensation has been used by Cannat *et al.* [1999] to estimate regional along-axis variations in mantle temperatures and in the thickness of the magmatic crust in this part of the SWIR, based on regional variations of axial depths. This model assumes homogeneous mantle compositions and neglects the cooling effect of transform faults. It suggests differences of $\sim 25^\circ\text{C}$ in subaxial mantle temperature and of ~ 1 km in magmatic crust thickness between the area east of Melville FZ, and the area between Atlantis II FZ and Gallieni FZ (Figure 2). The ridge west of Gallieni FZ is substantially shallower (average depth: 3100 m; Figure 2), suggesting significantly higher mantle temperatures and thicker magmatic crust [Cannat *et al.*, 1999].

[9] Variations in basalt Na_{8.0} contents (Na contents corrected from the effect of shallow crystal fractionation; [Klein and Langmuir, 1987]) are to first order consistent with melt supply variations inferred from regional axial depths. Basalts collected east of Melville FZ commonly have Na_{8.0} contents $>3.5\%$, suggesting very low values for the mean extent of melting of the subaxial mantle [Dick *et al.*, 1984; Price *et al.*, 1986; Robinson *et al.*, 1996; Humler *et al.*, 1998; Meyzen *et al.*, 2003]. The highest Na_{8.0} values are found in basalts dredged between 61° and 64°E , just east of the Melville FZ (Figures 1 and 2). By contrast, basalts collected between the Gallieni and Melville FZs generally have Na_{8.0} contents between 2.9 and 3.5 [Johnson and Dick, 1992; Robinson *et al.*, 1996; Humler *et al.*, 1998; Meyzen *et al.*, 2003], suggesting higher, yet still relatively small, mean

extents of mantle melting. Basalts collected to the east of Melville FZ are anomalously depleted in titanium and other moderately incompatible elements. The favored interpretation is that this depletion reflects a different, more depleted, mantle source east of Melville which acts as a major chemical boundary [Meyzen *et al.*, 2003].

[10] Ultramafics were recovered from 13 dredges, 7 to the east of Melville FZ, and 6 between Melville and Gallieni FZ (Figures 1 and 2). All ultramafic-bearing dredges but one (dredge 69) sampled the walls of the axial valley, in areas characterized by greater than average axial depths (Figure 2) and positive gravity anomalies (i.e., areas of thinner crust and/or denser mantle). Dredge 69 sampled the top of a broad ridge, within the axial valley, near Gazelle FZ. Table 1 gives a summary of the rock types recovered in each dredge, and their approximate proportions. Serpentinized harzburgites and lherzolites are, with basalts, the dominant lithologies. Three dredges (14, 21, and 23), all located between 63° and 65°E (Figure 2), contain both plagioclase-bearing, and plagioclase-free harzburgites. Dunites occur in 7 of the 13 dredges (Table 1). Serpentinized peridotites are occasionally cross-cut by pyroxenitic, gabbroic and basaltic dikes, but massive gabbros are generally not abundant. Basalts were recovered with peridotites in 10 of the 13 dredges; dredges 14 and 24 were almost empty, containing only small fragments and gravels of peridotites. The composition of the SWIR lithosphere in our study area, as sampled in dredge hauls, therefore appears dominantly bimodal, consisting primarily of basalts and residual mantle-derived peridotites. Dick [1989] reached the same conclusion for the SWIR lithosphere near transform faults, based on earlier dredges in the walls of SWIR fracture zones.

[11] For this paper, we selected 53 samples of plagioclase-free spinel lherzolites and harzburgites, representing the 13 peridotite-bearing dredges. These selected samples were cut away from dunite, pyroxenite, plagioclase or gabbro layers and dykes. As shown in the next sections, the spinel phase in these 53 samples contains less than 0.2 wt% TiO₂. Based on these criteria, these 53 selected samples are inferred to be residual [Dick, 1989; Seyler and

Table 1. Dredge Locations, Depths and Amounts of Mafic-Ultramafic Samples Recovered From the Edul Cruise

Dredge Number	Start Depth (m)	Latitude (°S)	Longitude (°E)	Lithologies (kg)			
				harzb-lherz	dunites	basalts	gabbros
3	5000	26.488	67.979	30	-	50	-
6	4900	26.98	67.221	5	3	250	-
14	5050	27.891	64.679	0.5	-	-	0.2
21	4800	27.99	63.503	250	10	60	40
23	4450	28.133	63.161	200	40	5	-
24	5000	28.404	62.592	0.1	-	-	-
25	4500	28.883	61.9425	300	2	6	-
42	5000	31.038	59.121	1	-	500	-
56	4200	34.025	55.828	700	-	5	200
59	3800	34.316	55.453	30	-	50	50
62	3900	34.467	54.9	500	10	200	6
64	4000	34.68	54.65	200	50	50	50
69	3850	36.1367	52.993	150	2	20	15

Bonatti, 1997; Kelemen *et al.*, 1997]. The petrography and mineral chemistry of dunites, plagioclase-bearing peridotites, and gabbros will be presented in a forthcoming paper.

3. Textures and Petrography

[12] Although samples are 60 to 90% serpentized, primary textures are still identifiable. Most samples have coarse-granular, transitional to porphyroclastic textures after small to moderate amounts of high-temperature recrystallization. Mylonites with elongated pyroxene porphyroclasts set in a fine grained matrix only occur in dredge 6. The coarse-granular mineral assemblage is made of olivine, orthopyroxene (opx), spinel and clinopyroxene (cpx), this latter phase being absent in some harzburgites. The dominant modal composition is close to the harzburgite - lherzolite boundary, with 4–6% cpx (Table 2 and Figure 3). In addition to porphyroclasts and recrystallized subgrains, most samples contain 1–2 vol.% late-stage minerals (cpx, spinel) in veins and in interstitial positions.

[13] Primary olivine and opx are coarse, up to 20 mm in size. Recrystallized grains of olivine (neoblasts) vary in size from 0.2 to 0.5 mm. Deformation in opx is marked by recrystallization into relatively large neoblasts (1–5 mm diameter), kink-bands boundaries and microfractures. Textural relationships between opx and olivine porphyroclasts are of two types. In one type, opx is highly irregular in shape, characterized by strongly resorbed grain

boundaries with deep embayments filled with recrystallized olivine. Frequently, the embayed olivine has developed subshape to euhedral shape at the contact with the opx. In the second type, opx is virtually unstrained, subequant in shape, with smooth curvilinear grain boundaries in contact with very coarse olivine grains showing undulose extinction and occasional recrystallization. In these samples, opx can be as large as 2 cm in diameter.

[14] Opx porphyroclasts display, in addition to thin cpx exsolution lamellae, inclusions of various shapes and sizes. The inclusions are dominantly cpx, then olivine, and spinel, occurring as individual grains, or in polymineral association, and varying in size from 0.1 to 1 mm (Figure 4a). Polymineral inclusions of cpx, pargasite, phlogopite and apatite have also been found in samples from dredge 23 [Seyler *et al.*, 2002]. Cpx inclusions are especially abundant (up to ~18 vol% of the opx host), coarse and euhedral when the opx hosts are coarse and subequant. Opx rich in inclusions and opx free of inclusion may coexist in a single thin section. Cpx in inclusions range in shape from euhedral to lamellar, and the distinction between exsolution and inclusion is not always clear. Magmatic twins are not exceptional, and all coarse cpx inclusions display thin exsolutions of opx.

[15] Spinel occurs as large grains (0.5–2 mm diameter), rather blocky in outline, near opx margins or disseminated within the olivine matrix. In many instances, these large spinels display irregularly

Table 2. Distribution of the 53 Samples Selected for This Study Into Four Petrographic Groups, Based on Visual (Semi-quantitative) Estimates of Modal Clinopyroxene (cpx) in Thin Section^a

Dredge	Studied EDUL peridotite samples				Total n = 53
	Harzburgite* 0.5–2% cpx	Harzburgite 1–4% cpx	Harz/Lherz 4–6% cpx	Lherzolite 6–9% cpx	
3		DR3-1			1
6		DR6A-1-1 DR6B-3-1	DR6A-1-2 DR6A-2-3 DR6B-3-2	DR6B-1-3	6
14		DR14-2-1	DR14-3-3		2
21		DR21-7-2 DR21-9-1	DR21-1-3 DR21-2-1 DR21-5-1 DR21-5-4	DR21-5-2 DR21-5-3	8
23	DR23-2-1	DR23-3-5	DR23-3-2	DR23-2-5	4
24			DR24-1		1
25			DR25-3-2 DR25-5-1 DR25-6-1	DR25-5-2	4
42	DR42-4-4	DR42-4-2 DR42-4-3			3
56			DR56-3-8 DR56-3-5 DR56-3-11		3
59		DR59-2-2			1
62		DR62-3-8 DR62-4-1	DR62-3-12 DR62-4-2 DR62-4-3 DR62-4-7		6
64			DR64-1-5 DR64-1-7 DR64-1-10 DR64-1-15 DR64-1-16		5
69	DR69-1-2 DR69-1-13 DR69-1-14 DR69-1-16 DR69-1-19	DR69-1-1 DR69-1-6 DR69-1-10 DR69-1-20			9

^a The 2 groups of harzburgites differ by lack of protogranular (or relict) clinopyroxene in harzburgite* while this cpx textural type is present in common harzburgites. Number of samples (n) is given.

shaped boundaries attesting to poikiloblastic overgrowth. In other instances, especially in harzburgites very poor in cpx, spinel porphyroclasts (re)equilibrated into subcrystals to euhedral crystals that poikilitically enclose tiny grains of olivine, opx and cpx. Vermicular spinel intergrown with opx neoblasts are frequently observed. Textural transitions from coarse vermicular to blocky then to euhedral shapes are suggested in some thin sections. In all cases, thin stringers of spinel migrate from the spinel grains along the interfaces of the olivine neoblasts or to fill cracks and veinlets that cross-cut the peridotite (Figure 4b).

[16] Protogranular cpx vary in size from coarse (up to 5 mm) in lherzolites to medium-sized in harzburgites. The coarser porphyroclasts are more strained (kink bands, and undulose extinction) than the smaller and have exsolved larger lamellae of opx. Very coarse cpx crystals in lherzolites commonly show two sets of exsolution lamellae. In contrast with opx porphyroclasts, cpx porphyroclasts are only exceptionally recrystallized into subgrains and are never affected by brittle deformation. Cpx porphyroclasts occurring in true lherzolites (e.g., modal cpx >6%) are comparable in size and shape to the opx porphyroclasts with which they are

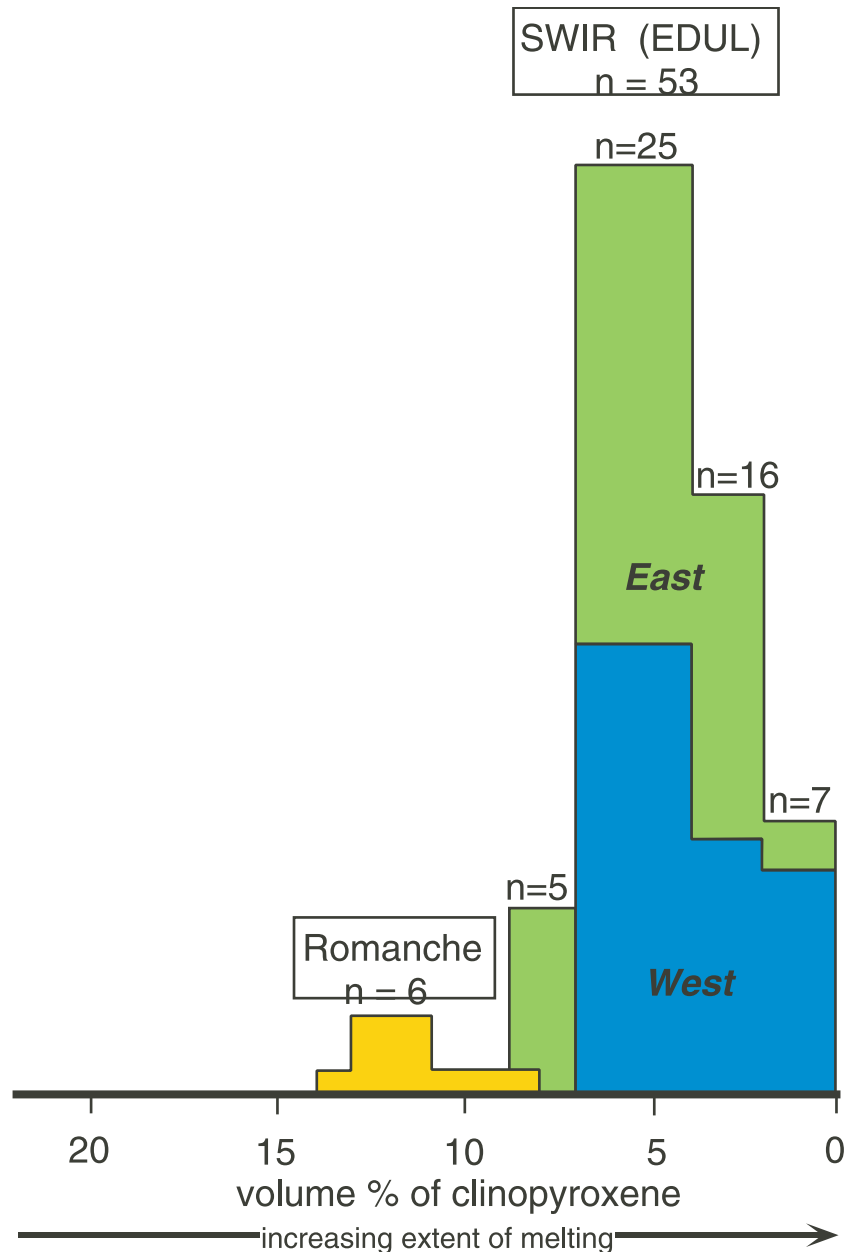


Figure 3. Histogram showing the abundance of clinopyroxenes in the 53 studied EDUL peridotite samples, west and east of Melville FZ. Data are taken from Table 2. Romanche peridotites in equatorial Atlantic ocean, known as the most fertile abyssal peridotites [Bonatti *et al.*, 1993], are displayed for comparison. Number of samples (n) is given.

associated, forming a pyroxene network enclosing very coarse areas of olivines. Contacts between opx and cpx grains are interlobed or curved. Smaller porphyroclasts are generally not associated with opx. They occur as discrete crystals or in clusters between the olivine grains. Within the clusters, cpx grains display curved grain boundaries or are frequently intergrown, with interpenetrative textures suggestive of magmatic crystallization (Figure 4c).

Contact between two cpx grains are often underlined by a reaction zone made of cpx, spinel and olivine neoblasts. Cpx porphyroclasts commonly display irregular, spongy rims enclosing small, recrystallized olivine grains. These rims are in apparent interconnection with tiny grains of cpx, of sinusoidal shape, scattered in the recrystallized olivine assemblage (Figure 4d). Cpx porphyroclasts also commonly grade into unstrained, elongated crystals or

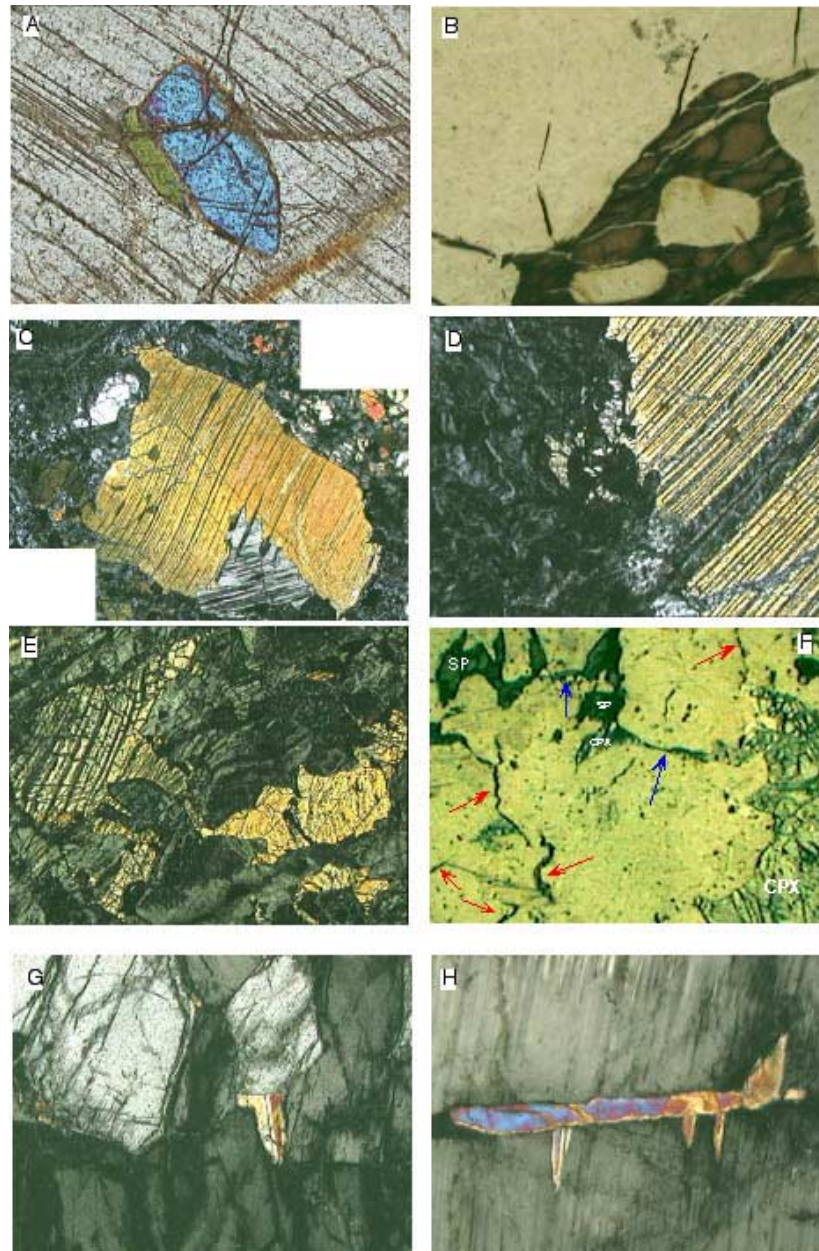


Figure 4. Microphotographies. (a) Inclusions of olivine (blue) and diopside (green) in subequant, coarse opx porphyroclast; crossed nichols; field length is 1.3 mm. (b) Stringers of spinel connected to poikilitic spinel at junctions of (serpentinized) olivine neoblasts; field length is 0.5 mm. (c) Cluster of two cpx showing interpenetrative texture; secondary opx blebs (in gray) developed at the contact; field length is 2 mm. (d) Intergranular, spongy cpx porphyroclast rims in optical continuity with tiny, grains of cpx, interstitial between (serpentinized) olivine neoblasts; field length is 3 mm. (e) Medium-sized cpx crystals interconnected by their deeply embayed margins, set within (serpentinized) olivine; field length is 4 mm. (f) Stringers and veinlets of cpx and spinel, both originating from large crystals, merging within (serpentinized) olivine. Red and blue arrows show spinel stringers and spinel + cpx veinlets across serpentinized olivine, respectively; field length is 2 mm. (g) Magmatic twinned cpx at the junction of opx subgrains; field length is 2 mm. (h) Cpx-filled microfracture within coarse opx grain; field length is 1.5 mm.

veinlets that cross-cut the olivine matrix (Figure 4e) or follow the intergranular spaces between olivine neoblasts. These veins of cpx can merge with the stringers and veinlets of spinel originated from spinel porphyroclasts, to form vermicular intergrowths or bi-mineral veinlets (Figure 4f).

[17] Such late-stage, small-sized grains of cpx and spinel are observed in almost all peridotite samples, including harzburgites that are devoid of cpx porphyroclasts. Late-stage cpx rim olivine, opx and the large spinels. Veinlets of cpx and spinel, separately or associated, fill cracks and cement broken opx porphyroclasts (Figures 4g and 4h). Fine-grained neoblastic assemblages of olivine and cpx with interstitial spinel \pm magmatic sulfide also surround some opx and cpx porphyroclasts, the latter frequently having a cloudy appearance. Small-sized cpx occasionally show magmatic twins; all have exsolved thin lamellae of opx but deformation depicted by bending of lamellae is exceptional. Cpx indeed show a continuum of size and shape that makes difficult to distinguish between small relict grains and late-stage crystals.

[18] In summary, textural features support a complex origin for the Edul peridotites. Most samples display high temperature, plastic deformation responsible for the formation of porphyroclasts. The ragged shapes of the cpx and spinel and the spatial association between spongy porphyroclast rims and intergranular and vein cpx and spinel suggest that this deformation occurred at solidus or near-solidus conditions. Similar cpx textures can be observed in experimental charges where grains of natural cpx set in a olivine matrix are partially molten [see *Falloon et al.*, 1999, Figure 6]. Furthermore, late-stage, magmatic cpx, spinel and sulfides bear witness of melt-present plastic recrystallization [*Seyler et al.*, 2001]. Cpx clusters and discrete, medium-sized cpx are characterized by shapes intermediate between relict and magmatic and are responsible for the modal heterogeneity of the peridotites. However, some samples show textures that are characteristic of high temperature annealing. Those contain preferentially the polymineral inclusions. Temporal relation between deformed and annealed samples remains unclear, but is nether-

theless suggestive of a stage of high temperature re-equilibration at spinel stability condition.

4. Mineral and Whole Rock Chemistry

4.1. Mineral Chemistry

[19] Electron microprobe analyses of the mineral phases were performed in the 53 selected samples, using the automated CAMECA-CAMEBAX electron microprobe of the CAMPARIS micro-analysis center (University of Paris 6). Analytical conditions are 15kV accelerating voltage, 20 and 40 nA beam current, 20–40s count times, and a focused beam. Natural mineral standards were used for calibration. Detection limits are within 0.01–0.03 wt.%. Between 1 and 8 thin sections per sample have been analyzed but no difference has been observed for mineral chemistry between several thin sections in the same sample. Mineral compositions are listed in Tables 3 to 6. EDUL mineral compositions are compared to Mid Atlantic Ridge (MAR) peridotites collected in the MARK area [*Ghose et al.*, 1996; *Komor et al.*, 1990; *Stephens*, 1997].

4.1.1. Olivine

[20] No fresh olivine remains in dredge 69 peridotites. In the other 12 dredges, olivine grains are unzoned and within-sample and within-dredge variations in Fo are less than 0.5%. Fo contents range from 89.28 to 90.73. NiO contents range from 0.32 to 0.43 wt%, with no systematic correlation with Fo.

4.1.2. Orthopyroxene

[21] Orthopyroxene porphyroclasts display large, intragrain and intergrain compositional variations. In a single thin section, the cores of the largest grains (>8 mm) are enriched in Al, Cr, Ca with respect to the rims, and to the core of smaller grains (Figure 5). Core-rim variations in Al₂O₃ and Cr₂O₃ (Figure 5a) contents do not significantly modify Cr/(Cr + Al) ratio (= Cr#). CaO contents display a large range of core to rim variations (Wo 1–5%). In Na-rich opx, Na₂O contents increase with CaO contents (Figure 5b). Mg/(Mg + Fe) ratios (= Mg#) show no correlation with CaO. TiO₂ contents are low (<0.2%) but also display a weak tendency to

Table 3. (Representative Sample) Compositions of Olivines From the Edul Cruise Spinel Lherzolites and Harzburgites^a [The complete Table 3 is available in the HTML version of the article at <http://www.g-cubed.org>.]

Sample Number	DR3-1		DR6A-1-1		DR6A-1-2		DR6B-1-3		DR6B-3-1		DR6B-3-2		DR21-1-3		DR21-2-1		DR21-5-1	
	Average	±	Average	±	Average	±	Average	±	Average	±	Average	±	Average	±	Average	±	Average	±
SiO ₂	40.97	0.37	40.86	0.11	40.81	0.21	40.58	0.11	40.44	0.09	41.27	0.21	41.23	0.16	40.74	0.19	40.95	0.16
FeO	9.17	0.36	9.52	0.12	9.26	0.31	9.86	0.22	10.23	0.12	10.33	0.42	9.47	0.46	9.46	0.13	9.35	0.01
MnO	0.14	0.03	0.12	0.03	0.13	0.02	0.13	0.04	0.15	0.03	0.13	0.07	0.12	0.16	0.13	0.08	0.19	0.17
NiO	0.43	0.09	0.35	0.04	0.41	0.05	0.41	0.02	0.33	0.03	0.4	0.1	0.37	0.02	0.36	0.02	0.41	0.06
MgO	49.66	0.87	49.24	0.05	49.32	0.31	49	0.24	48.35	0.14	48.6	0.4	49.36	0.03	48.77	0.18	50.14	0.35
CaO	0	0.01	0.02	0.01	0.03	0.01	0.02	0.02	0.06	0.03	0.07	0.12	0.06	0.06	0.04	0	0.06	0.04
Total	100.37	1.44	100.1	0.19	99.95	0.23	100	0.35	99.57	0.31	100.79	0.2	100.6	0.04	99.5	0.39	101.1	0.04
Fo%	90.61	0.29	90.22	0.12	90.47	0.33	89.85	0.21	89.38	0.09	89.35	0.44	90.29	0.43	90.19	0.13	90.53	0.07

^a Average of 5–10 electron microprobe analyses per sample.

decrease from core to rim of individual opx grains, and to be lower in small grains. All these variations are thought to result from diffusion processes with uncomplete reequilibration during cooling of the peridotites into the SWIR lithosphere.

[22] To discuss intersample variations, we first averaged the core compositions of the largest porphyroclasts (>0.8 mm in size) in each sample. Then, for each dredge, the average composition of samples has been considered, as displayed in Figure 6. Dredge 6 samples can be divided into two compositional groups, referred to as 6a and 6b, on the basis of their mineral chemistry. In a Cr₂O₃ versus Al₂O₃ diagram (Figure 6a), 12 of the 13 dredges define a nearly linear trend. This suggests that opx porphyroclast cores in these dredges equilibrated in roughly similar pressure-temperature conditions. The only exception is dredge 6; these samples are also the only ones in our set with porphyroclastic to mylonitic textures indicative of strong deformation in the ductile part of the SWIR lithosphere. These opx compositions suggest Al- and Cr-loss even in the porphyroclast cores due to re-equilibration at lower temperature during mylonitization. Average opx Cr# ratios increase regularly from 6.9 to 15.6 along the Cr₂O₃ versus Al₂O₃ trend, suggesting increasing amounts of melt extraction (Figure 6a). Average opx Mg# vary from 89.29 to 92.27 (Figure 6b), with intradredge variations <0.5%. With the exception of dredges 24 and 69, interdredge variations are of the same order (90.26 ± 0.27), resulting in a weak correlation between Cr# and Mg#. The field of Cr# versus Mg# overlaps well with that of MAR samples from the MARK area. Samples from dredge 69 do, however, plot outside this trend, at higher Mg# values (Figure 6b). The olivine - opx partition coefficient for Fe-Mg is close to unity (0.998 ± 0.003) in all samples, consistent with an equilibrium at high temperatures. Opx TiO₂ contents decrease with increasing Cr# (Figure 6c), as expected for increasing degrees of melting. Average opx compositions for dredges 14, 23 and 42 plot above the TiO₂ versus Cr# trend for opx from the MARK area. Opx Na₂O contents also tend to decrease with increasing Cr#, but with some scattering. Although opx

Table 4. (Representative Sample) Compositions of Orthopyroxenes From the Edul Cruise Spinel Lherzolites and Harzburgites^a [The complete Table 4 is available in the HTML version of the article at <http://www.g-cubed.org>.]

Sample Number	DR3-1		DR6A-1-1		DR6A-1-1		DR6A-1-2		DR6B-1-3		DR6A-2-3		DR14-2-1		DR14-2-1	
	Core Average	±	Core Average	±	rim Average	±	Core Average	±	rim Average	±						
SiO ₂	55.15	0.86	54.97	0.74	55.49	0.89	55.69	0.23	54.51	0.27	55.76	0.39	54.33	0.19	55.33	0.22
TiO ₂	0.05	0.06	0.06	0.02	0.05	0.02	0.05	0.02	0.09	0.01	0.06	0.01	0.12	0.02	0.11	0.02
Al ₂ O ₃	4.30	0.42	3.65	0.22	2.94	0.15	3.43	0.24	4.49	0.23	3.22	0.19	4.54	0.19	3.92	0.34
Cr ₂ O ₃	0.88	0.02	0.91	0.09	0.65	0.13	0.75	0.10	0.70	0.07	0.82	0.07	0.87	0.03	0.72	0.08
FeO	5.81	0.28	6.12	0.23	6.26	0.05	6.16	0.13	6.34	0.11	5.93	0.10	6.19	0.11	6.48	0.08
MnO	0.14	0.09	0.14	0.04	0.14	0.02	0.13	0.04	0.14	0.03	0.14	0.06	0.14	0.02	0.18	0.02
NiO	0.10	0.05	0.10	0.05	0.05	0.03	0.09	0.02	0.10	0.03	0.07	0.02	0.10	0.03	0.10	0.04
MgO	32.49	1.17	32.08	0.77	32.79	0.42	32.79	0.41	31.89	0.35	33.12	0.21	31.99	0.43	32.61	0.24
CaO	1.87	0.59	1.68	0.99	1.00	0.23	1.32	0.36	1.51	0.38	1.16	0.12	1.27	0.53	1.12	0.38
Na ₂ O	0.06	0.03	0.09	0.05	0.06	0.02	0.06	0.03	0.06	0.02	0.08	0.01	0.03	0.02	0.02	0.01
Total	100.83	1.57	99.80	0.62	99.44	1.55	100.46	0.23	99.82	0.36	100.34	0.35	99.57	0.21	100.58	0.23
Wo	3.64	1.23	3.30	1.96	1.94	0.44	2.55	0.71	2.97	0.75	2.22	0.24	2.51	1.06	2.17	0.72
En	87.39	1.13	87.15	1.72	88.38	0.42	87.98	0.64	87.10	0.71	88.66	0.17	87.75	0.97	87.77	0.73
Fs	8.97	0.35	9.55	0.32	9.67	0.07	9.46	0.18	9.93	0.16	9.12	0.18	9.73	0.12	10.06	0.12
Mg#	90.89	0.27	90.33	0.21	90.33	0.08	90.47	0.18	89.96	0.13	90.88	0.13	90.21	0.10	89.97	0.15
Cr#	12.13	0.96	14.36	1.22	12.83	2.00	12.70	0.87	9.43	0.41	14.52	0.40	11.42	0.35	10.91	0.28

^a Average of 5–10 electron microprobe analyses per sample.

Table 5. (Representative Sample) Compositions of Clinopyroxenes From the Edul Cruise Spinel Lherzolites and Harzburgites^a [The complete Table 5 is available in the HTML version of the article at <http://www.g-cubed.org>.]

	DR03-1		DR06A-1-1		DR06A-1-1		DR06A-1-1		DR06A-1-2		DR06B-1-3		DR06A-2-3		DR06A-2-3		DR06B-3-1	
	Core	Inclusions	Core	Inclusion	Late	Core	Core	Core	Core	Core	Core	Inclusions	Core	Inclusions	Core	Inclusions	Core	Core
	Average	±	Average	±	Average	±	Average	±	Average	±	Average	±	Average	±	Average	±	Average	±
SiO ₂	51.40	0.44	50.28	0.37	52.36	0.12	52.04	0.28	50.74	0.31	50.81	0.22	52.63	0.12	52.97	0.49	50.93	0.08
TiO ₂	0.07	0.03	0.09	0.05	0.14	0.01	0.15	0.01	0.28	0.02	0.33	0.02	0.18	0.02	0.17	0.02	0.24	0.01
Al ₂ O ₃	5.91	0.13	5.23	0.07	4.90	0.26	4.94	0.36	5.90	0.29	5.89	0.07	4.36	0.34	4.21	0.36	6.35	0.05
Cr ₂ O ₃	1.48	0.20	1.35	0.04	1.72	0.16	1.50	0.16	1.24	0.04	1.26	0.06	1.62	0.12	1.55	0.15	1.27	0.06
FeO	2.65	0.07	2.26	0.15	2.68	0.15	2.74	0.19	2.99	0.11	2.61	0.25	2.60	0.04	2.58	0.04	3.11	0.03
MnO	0.09	0.08	0.09	0.03	0.08	0.03	0.12	0.08	0.11	0.02	0.06	0.02	0.11	0.03	0.10	0.03	0.13	0.01
NiO	0.10	0.09	0.03	0.04	0.05	0.02	0.05	0.02	0.06	0.04	0.02	0.01	0.05	0.01	0.04	0.01	0.03	0.01
MgO	15.72	0.32	15.43	0.27	15.52	0.43	16.04	0.71	16.03	0.48	15.40	0.99	16.17	0.63	16.05	0.40	15.07	0.00
CaO	22.57	0.23	22.53	0.60	20.90	0.38	20.66	0.95	21.12	0.43	22.05	1.34	20.72	0.31	20.92	0.39	21.71	0.01
Na ₂ O	0.64	0.03	0.72	0.03	1.15	0.09	0.93	0.05	0.64	0.08	0.69	0.00	1.18	0.04	1.17	0.03	0.68	0.04
Total	100.63	0.61	98.01	1.04	99.49	0.36	99.17	0.24	99.09	0.39	99.11	0.18	99.59	0.06	99.75	0.21	99.51	0.28
Wo	48.46	0.67	49.17	1.04	46.82	1.21	45.71	2.20	46.09	1.92	48.41	3.18	45.73	1.26	46.15	0.99	48.03	0.01
En	46.94	0.75	46.82	1.02	48.36	0.95	49.35	1.92	48.65	1.62	47.01	2.80	49.61	1.31	49.24	0.95	46.38	0.04
Fs	4.60	0.20	4.01	0.02	4.83	0.26	4.94	0.32	5.26	0.39	4.58	0.38	4.66	0.05	4.61	0.10	5.59	0.06
Mg#	91.35	0.28	92.41	0.06	91.16	0.23	91.26	0.35	90.54	0.45	91.33	0.25	91.73	0.19	91.73	0.11	89.62	0.08
Cr#	14.35	1.79	14.78	0.97	19.05	0.89	16.93	0.58	12.35	0.36	12.50	0.37	19.90	0.05	19.74	0.30	11.83	0.38

^a Average of 5–10 electron microprobe analyses per sample for porphyroclast Cores and relicts; 1 to 5 analyses per sample for Inclusions.

Table 6. (Representative Sample) Compositions of Spinels From the Edul Cruise Spinel Lherzolites and harzburgites^a [The complete Table 6 is available in the HTML version of the article at <http://www.g-cubed.org>.]

Sample	DR3-1	DR6A-1-1	DR6A-1-2	DR6B-1-3	DR6A-2-3	DR6B-3-1	DR6B-3-2	DR14-2-1	DR14-3-3	DR21-1-3	DR21-2-1	DR21-5-1	DR21-5-2
Number	Average ±	Average ±	Average ±	Average ±	Average ±	Average ±	Average ±	Average ±	Average ±	Average ±	Average ±	Average ±	Average ±
SiO ₂	0.01 0.01	0.02 0.01	0.02 0.01	0.02 0.02	0.03 0.01	0.02 0.01	0.02 0.03	0.04 0.02	0.06 0.03	0.02 0.03	0.02 0.01	0.01 0.02	0.02 0.02
TiO ₂	0.02 0.01	0.10 0.02	0.07 0.01	0.10 0.02	0.10 0.04	0.12 0.03	0.12 0.03	0.09 0.01	0.14 0.04	0.09 0.01	0.08 0.01	0.08 0.02	0.07 0.06
Al ₂ O ₃	47.32 0.25	35.46 1.33	40.61 0.74	48.75 0.96	34.97 2.86	46.65 1.04	45.85 2.00	46.08 1.30	44.41 1.23	47.45 1.10	49.03 0.39	53.24 0.37	52.58 0.69
Cr ₂ O ₃	21.40 0.36	30.13 1.59	26.27 0.60	17.23 0.96	30.91 3.51	19.98 0.79	20.61 0.47	21.44 1.30	21.66 1.00	19.79 0.74	19.12 0.38	13.91 0.22	15.44 0.74
Fe ₂ O ₃	1.96 0.17	3.83 0.42	2.34 0.24	2.41 0.48	3.81 0.21	2.13 0.46	2.64 1.98	1.01 0.38	2.92 0.63	1.15 0.30	0.41 0.18	1.87 0.97	0.96 0.35
FeO	11.76 0.03	14.58 0.84	13.37 0.62	13.24 0.47	14.59 0.76	13.40 1.44	13.48 1.61	12.87 0.29	13.72 0.54	12.83 0.30	11.90 0.29	11.29 0.50	11.91 0.78
MnO	0.19 0.15	0.18 0.05	0.15 0.06	0.17 0.05	0.17 0.03	0.18 0.06	0.13 0.08	0.13 0.04	0.19 0.11	0.13 0.07	0.14 0.02	0.16 0.06	0.16 0.08
MgO	18.04 0.08	14.72 0.63	16.02 0.48	16.89 0.42	14.74 0.66	16.68 1.06	16.63 1.21	16.87 0.28	16.32 0.41	17.02 0.33	17.77 0.20	18.68 0.12	18.3 0.61
NiO	0.30 0.09	0.19 0.06	0.20 0.05	0.31 0.04	0.18 0.02	0.22 0.03	0.25 0.09	0.25 0.03	0.24 0.09	0.23 0.14	0.25 0.03	0.36 0.08	0.28 0.09
Sum	100.98 0.48	99.08 0.49	98.85 0.20	98.81 0.27	99.31 0.76	99.16 0.34	99.48 0.64	98.76 0.29	99.67 0.92	98.72 0.11	98.72 0.16	99.60 1.71	99.72 0.46
Cr#	23.27 0.40	36.31 2.06	30.26 0.84	19.17 1.15	37.24 4.56	22.32 1.07	23.18 0.73	23.80 1.59	24.66 1.37	21.86 1.03	20.73 0.45	14.91 0.29	16.45 0.75
Mg#	73.22 0.14	64.27 2.30	68.10 1.67	69.46 1.28	64.28 2.20	68.90 3.69	68.70 4.14	70.04 0.81	67.95 1.38	70.28 0.86	72.69 0.70	74.69 0.86	73.24 1.94

^aAverage of 5–10 electron microprobe analyses per sample.

from dredges 56, 59, 62 and 64 have Na₂O close to or below detection limit (<0.03 wt.%), they are more depleted in Na than the opx from the other dredges (Figure 6d). Samples from dredges 3, 6, composition A, and 69 contain opx with both high Cr# and high Na₂O contents, and samples from dredges 6, composition B, and 23 are variably enriched in Na₂O with respect to Cr#.

4.1.3. Clinopyroxene

[23] Clinopyroxenes display a large range of intra-sample compositional variations at thin section scale. The relationships between these intrasample compositional variations, and the texture of cpx grains is illustrated in Figure 7 by two samples that have contrasting cpx compositions. Cpx porphyroclasts are strongly zoned for Al₂O₃ and Cr₂O₃, both oxides decreasing from core to rim, and between the cores of large and smaller grains (small porphyroclasts and interstitial grains; Figure 7a). This core-rim decrease in Al and Cr has a small effect on Cr# (Figure 7b), but Mg# is distinctly higher in rims than in cores. CaO contents do not vary from cores to rims and have a restricted range (21–24 wt%). Exceptional, low CaO values (down to 18 wt%) are however found in the cores of a few very large grains, in association with the highest Al₂O₃ and Cr₂O₃ concentrations, suggesting that the zoning is, like in opx, related to diffusion process during cooling. Na₂O and TiO₂ contents do not vary from cores to rims in porphyroclasts (Figures 7c and 7d). However, the more extreme border of some grains is slightly impoverished in Na and Ti. Compositions of the intergranular and vein-forming cpx vary in the same range as those of the porphyroclast rims.

[24] Clinopyroxene inclusions in opx also display large Al₂O₃ and Cr₂O₃ variations at thin section scale (Figure 7a). The highest concentrations in Cr₂O₃ in a given sample are commonly found in inclusions (e.g., in sample 64-1-7; Figure 7a). Cpx in inclusions are also frequently enriched in Na₂O and TiO₂ with respect to cpx porphyroclasts (Figures 7c and 7d). Cpx grains which are enclosed in coarse (up to 2 cm) opx are partic-

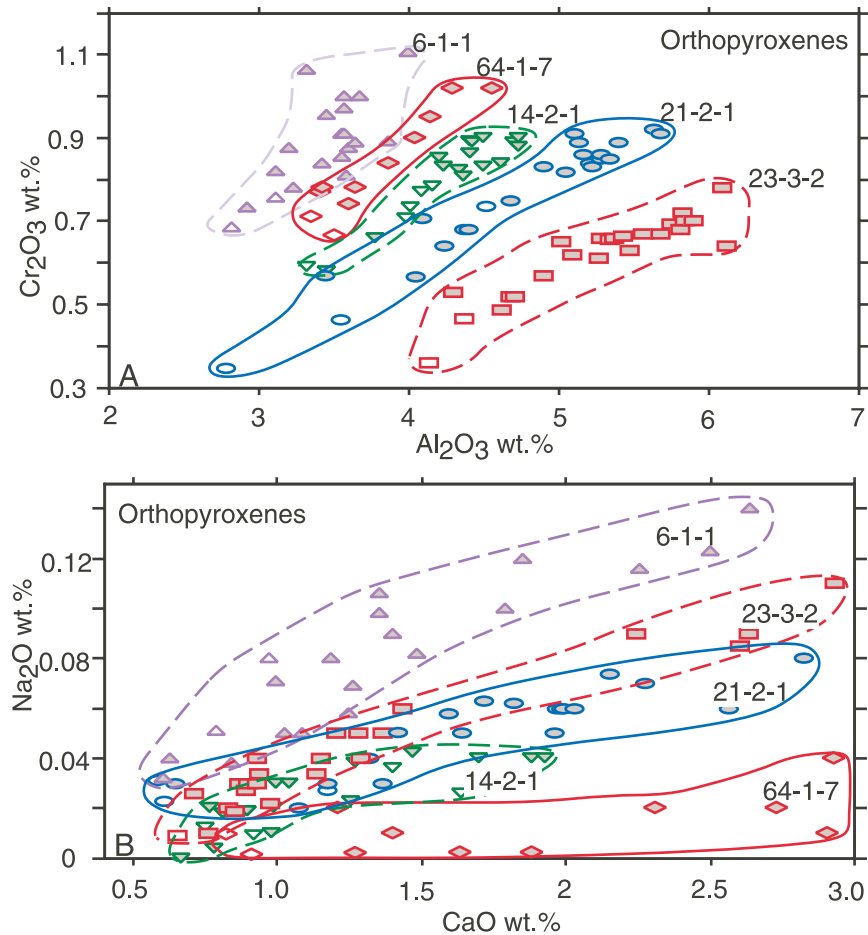


Figure 5. Examples of intragrain and intergrain compositional variations of the orthopyroxene within five representative samples. Filled symbols, porphyroclast cores; open symbols, porphyroclast rims.

ularly remarkable for their relatively large size and fertile compositions. For instance, cpx inclusions in dredge 23 contain Na₂O = 1.2–1.4 wt% and TiO₂ ~0.57 wt%, while rock-forming cpx contain Na₂O = 0.6–0.8 wt% and TiO₂ ~0.3–0.4 wt%.

[25] Core compositions of associated cpx and opx porphyroclasts are well correlated for Cr# ($\text{Cr\#}_{\text{opx}}/\text{Cr\#}_{\text{cpx}} = 0.82 \pm 0.05$) and Mg# ($\text{Mg\#}_{\text{opx}}/\text{Mg\#}_{\text{cpx}} = 0.992 \pm 0.005$). The $\text{Mg\#}_{\text{olivine}}/\text{Mg\#}_{\text{cpx}}$ is close to unity ($= 0.990 \pm 0.005$). The average compositions of cpx porphyroclast cores in each dredge are reported in Figure 8. Dredge 6 is represented, as in Figure 6, by two average compositions, referred to as 6A and 6B, because it does present a bimodal compositional distribution for all the mineral phases. Average cpx compositions in abyssal

spinel-peridotites from the Romanche FZ in the Atlantic, representing fertile end-member [Bonatti *et al.*, 1993], is also plotted in Figure 8.

[26] Average cpx Cr# increase (from 8.9 to 18.9) with increasing Cr₂O₃ (1 to 1.6 wt%) and decreasing Al₂O₃ (from 7 to 4.5 wt%), but cpx in dredges 3, 6, composition A, and 69 are enriched in Cr₂O₃ relative to Al₂O₃ (Figure 8a). With increasing Cr#, Mg# increase (from 89.6 to 92.8) and TiO₂ contents decrease (from 0.45 to 0.07 wt%) (Figures 8b and 8c). Cpx from dredges 6, 14, 21, 23, 24, 42 and 69 plot above the TiO₂ versus Cr# trend of MARK samples, having higher TiO₂ contents for a given Cr# (Figure 8c). Cpx Na₂O contents also tend to decrease at increasing Cr#, but display a large range of variation (from 0.1 to 1.4 wt%) that is not simply correlated with Cr#. In

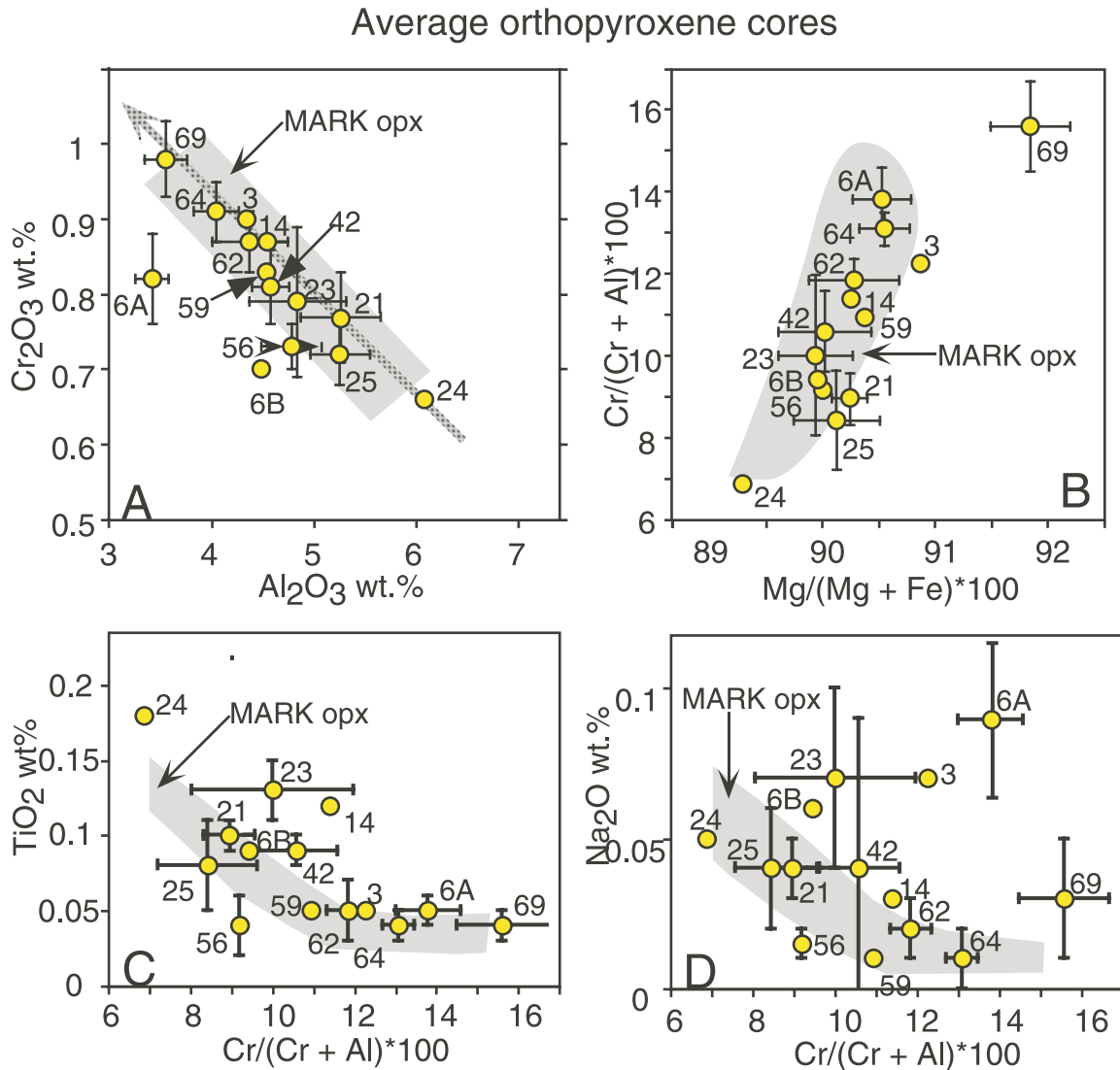


Figure 6. Average compositions and standard deviation of orthopyroxene porphyroclast cores for each dredges. Arrow indicates decreasing fertility in relation with increasing partial melting and melt extraction. Field in gray represents orthopyroxene compositions of MARK area (Mid Atlantic Ridge South of Kane Fracture Zone) peridotites [Komor et al., 1990; Ghose et al., 1996; Stephens, 1997].

particular cpx from dredges 6, composition A, and 69 have high Cr# and high Na₂O contents (Figure 8d). Except for the three dredges 25, 56 and 64, cpx Na₂O contents in EDUL samples are higher, at a given Cr# value, than those measured in cpx from the MARK area (Figure 8d). Na/Ti ratios in cpx from the EDUL dredges are higher than in cpx from the MARK area, particularly in cpx from dredges 3, 6, composition A, and 69 (Figure 9). High Na/Ti ratios (>10) are also observed in individual cpx grains from dredge 62. Compared with cpx from the MARK area, cpx from EDUL

dredges, particularly from those dredges located to the east of the Melville FZ, have higher Al^{VI}/Al^{IV} ratios (Figure 10a) associated with higher Na₂O contents (Figure 10b), and therefore appear enriched in the jadeite component.

4.1.4. Spinel

[27] Spinel grains from individual samples are homogeneous within analytical errors, with less than 15% intragrain and intergrain compositional variations for Cr# and Mg#. In the whole Edul

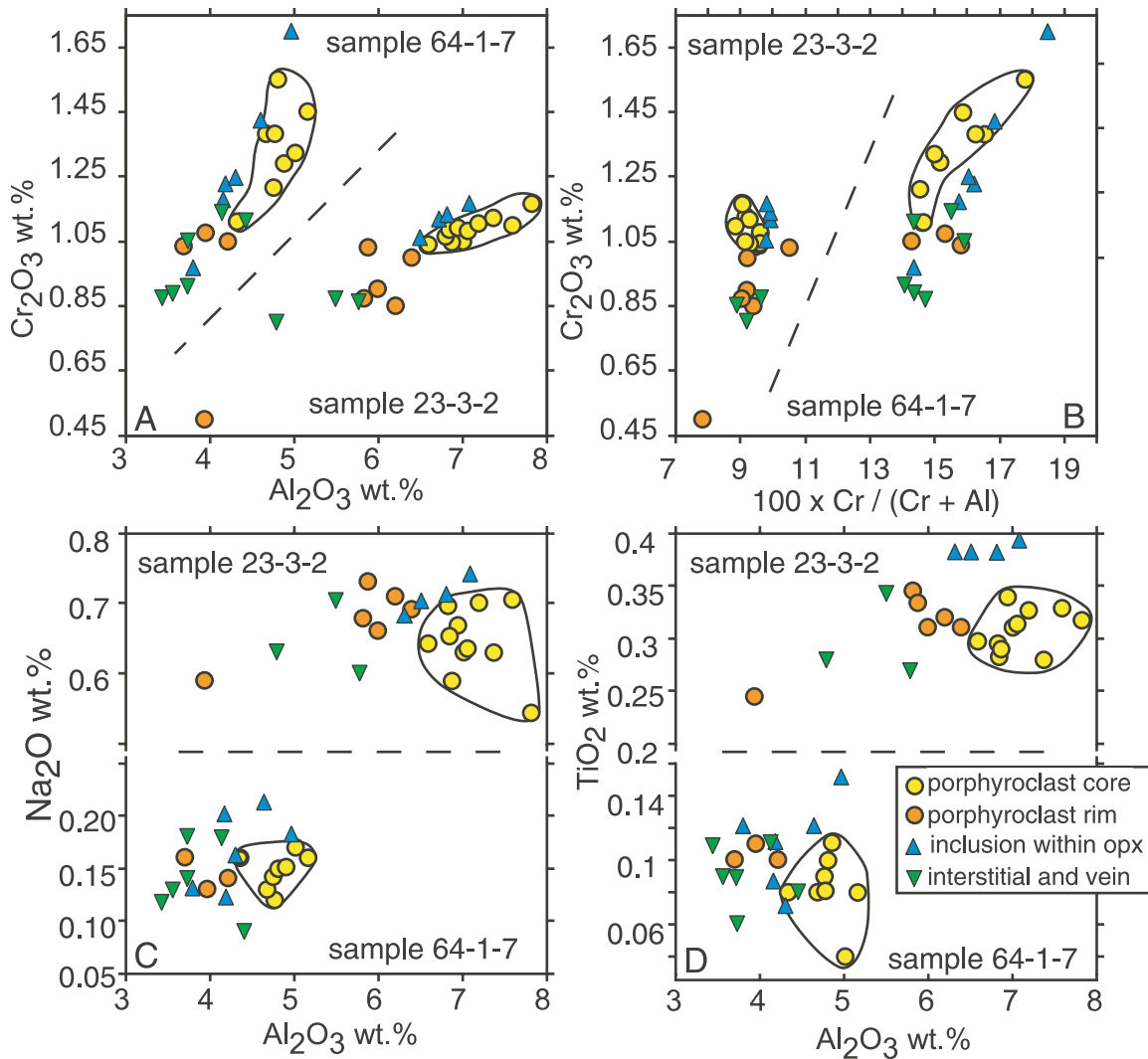


Figure 7. Examples of intragrain and intergrain compositional variations of clinopyroxene within two samples chosen for their extreme difference of composition. Fields of porphyroclast cores are circled.

area, average Cr# and Mg# per sample vary from 15.1 to 51.1 and 62 to 76, respectively. These two ratios show the usual, negative correlation characteristic of abyssal, plagioclase-free peridotite spinels. Average TiO₂ contents are ≤ 0.2 wt% in all samples, and ≤ 0.1 wt% in 75% of the sample set. Spinels that are included in opx are more aluminous than spinels belonging to the granular assemblages of the same samples (Cr# ~ 0.14 and 0.12 for the inclusions and Cr# ~ 0.25 and 0.27 for the matrix grains in dredges 23 and 62, respectively).

[28] Spinel composition is well correlated with the associated silicates. Olivine Fo content is

poorly correlated with spinel Cr#. Most EDUL dredges do, however, plot within the olivine Fo content versus spinel Cr# field of Atlantic peridotites (Figure 11). Dredge 69 plots well outside this trend, at significantly higher Fo contents (in the absence of preserved olivine, Fo content in this dredge was inferred from the Mg# of opx, using a Mg-Fe partition coefficient of 0.998).

4.2. Along-Axis Variations in Mineral Chemistry

[29] Selected mineral chemistry parameters (olivine Mg#, spinel Cr# and cpx TiO₂, Na₂O and

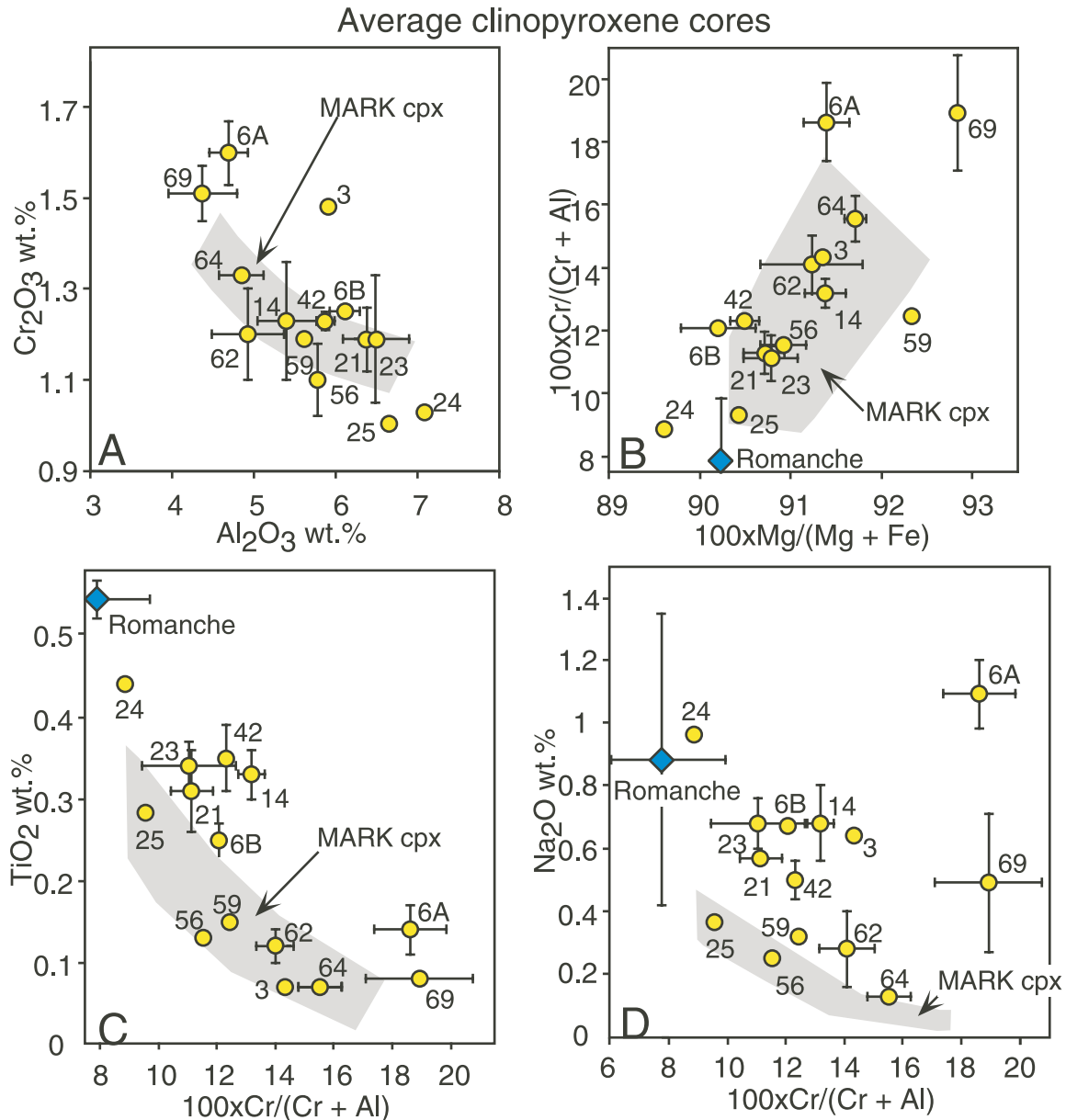


Figure 8. Average compositions and standard deviation of clinopyroxene porphyroclast cores for each dredges. Same legend as Figure 6. In addition, blue diamond are spinel-llerszolites from the Romanche Fracture Zone, Atlantic ocean [Seyler and Bonatti, 1997].

Na/Ti contents) have been reported as a function of longitude to describe the along-axis variations of mineral composition in these dredged peridotites (Figure 12). Mineral Mg# and Cr# and cpx TiO₂ contents are commonly used as indicators of fertility and partial melting, Mg# and Cr# correlating positively, whereas cpx TiO₂ contents vary in the opposite way. Na₂O content in cpx decreases with increasing partial melting extent.

Variations of these parameters along the EDUL section must show similar correlations if the mantle is simply residual of variable extents of melting of a homogeneous source composition. Peridotites from earlier dredges at the Atlantis II FZ/ridge intersection (~57°E, site 6 [Johnson and Dick, 1992]) have mineral compositions in good agreement with those of neighboring EDUL peridotites (Figure 12).

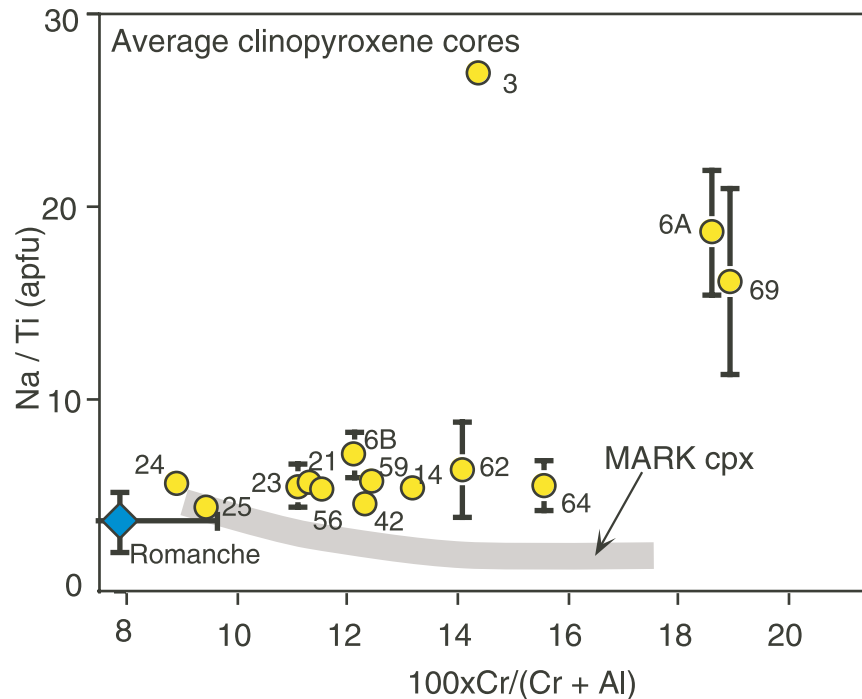


Figure 9. Average and standard deviation Na/Ti (cation per formula unit) ratios in clinopyroxene porphyroclast cores for each dredges. Same legend as Figure 8.

[30] At a broad scale, olivine Mg#, spinel Cr# and cpx TiO₂ show similar along-axis variations (Figures 12a, 12b, and 12c). East of Melville, there is an overall trend of decreasing spinel Cr# and increasing cpx TiO₂ from 67–68°E to 62–65°E. However, in detail, compositional variations are

very irregular and correlations display numerous anomalies, as illustrated by the following examples. Minerals in the two easternmost dredges seem to have random compositions. Dredge 3 minerals have moderate Cr# and Mg#, but cpx TiO₂ contents are very low. Dredge 6 is bimodal. Minerals

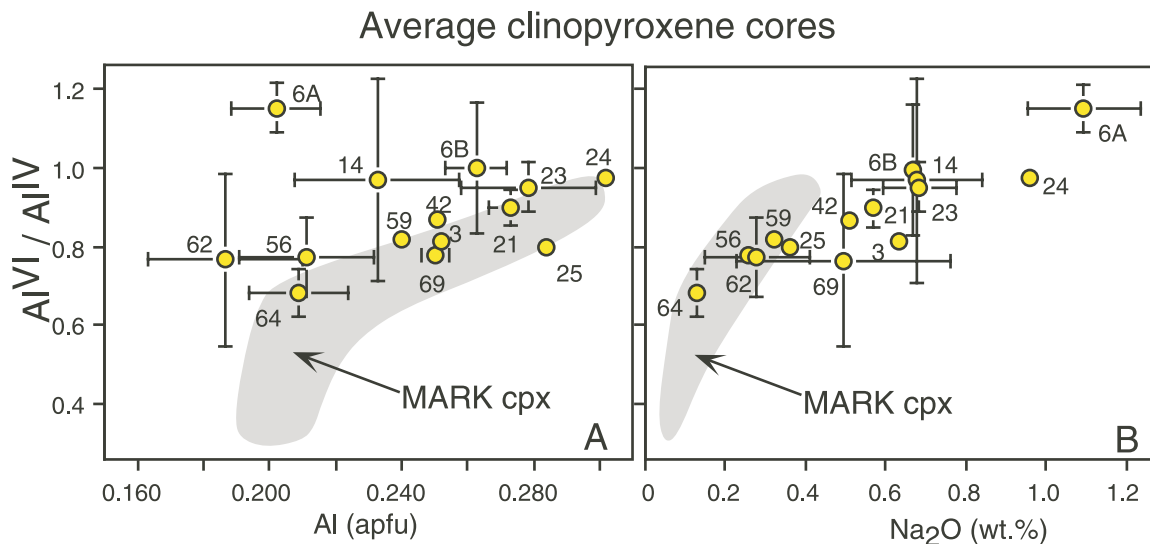


Figure 10. Average and standard deviation Al^{VI}/Al^{IV} ratios versus (a) Al (atom per formula unit) and versus (b) Na₂O (wt.%) in EDUL clinopyroxene porphyroclast cores. Same symbols as in Figure 8.

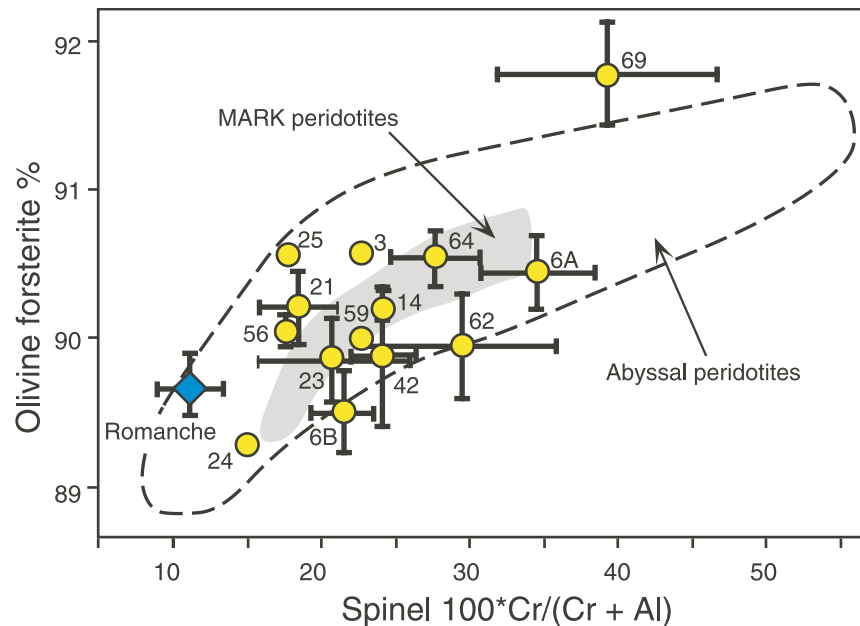


Figure 11. Olivine forsterite content versus spinel $100 \cdot \text{Cr}/(\text{Cr} + \text{Al})$ ratio (average and standard deviation per dredge) in EDUL peridotite samples. Same legend as Figure 8. Field of abyssal peridotites (other than MARK peridotites) are from *Dick* [1989], *Bonatti et al.* [1992] and *Michael and Bonatti* [1985].

of 6A have Mg# as high as in dredge 3 sample, but Cr# are much higher and cpx TiO₂ contents not as low. Minerals of 6B differ from 6A by lower Mg# and Cr# and higher cpx TiO₂ contents; samples 6B thus appear significantly more fertile than samples 6A. Dredges 14, 21 and 23 have broadly similar mineral compositions, although slightly fluctuating. Compared to samples 6B, the cpx of these dredges are richer in TiO₂, but the minerals have nevertheless similar Cr# while Mg# are significantly higher. Dredge 24 has the most fertile mineral compositions of the EDUL set, characterized by very low Mg# and Cr# and very high cpx TiO₂ contents. This dredge could thus be representative of the least melted mantle from the EDUL area. Dredge 25, just west of dredge 24, marks a significant increase in the degree of depletion, its minerals having higher Mg#, Cr# and lower cpx TiO₂. East of Atlantis II, there is a general trend of decreasing fertility, marked by increases in Mg# and Cr# and a decrease in cpx TiO₂ contents. Again, inconsistent and irregular variations in mineral compositions occur at a smaller scale in this region. Dredge 62 minerals have Cr# slightly too high with respect to Mg# and cpx TiO₂ contents. By contrast, dredge 56 minerals (and also

from the Atlantis II FZ peridotites) have low spinel Cr# and pyroxene Cr₂O₃ contents (Figures 6a and 8a) relative to the adjacent dredges. Dredge 69 minerals have the most refractory compositions, with very high Mg# and Cr#, though dredge 64 has slightly lower cpx TiO₂. Between Melville and Atlantis II FZ, dredge 42 is not well correlated with the nearest dredge, with moderate Mg#, but relatively high spinel Cr# and high cpx TiO₂.

[31] The cpx Na₂O general trend does not agree with the preceding indicators. It slightly decreases westward to reach minimum concentrations in dredge 64 (Figure 12d) and goes up again in dredge 69. With its very high cpx Na₂O content, dredge 24 departs from this general trend. However, because it also has a high cpx TiO₂ content, the Na/Ti ratio is similar to most EDUL cpx (Figure 12d). Moreover, high cpx Na₂O and TiO₂ correlate with low Mg# and Cr#. This could reflect a very fertile composition. By contrast, high Na₂O contents in cpx 6A and Na₂O well above the general trend in cpx 69 do not correlate with more fertile mineral compositions. Strong Na₂O - TiO₂ decoupling result in high Na/Ti ratios (Figure 12e). This is also obvious in dredge 3, where cpx have Na₂O con-

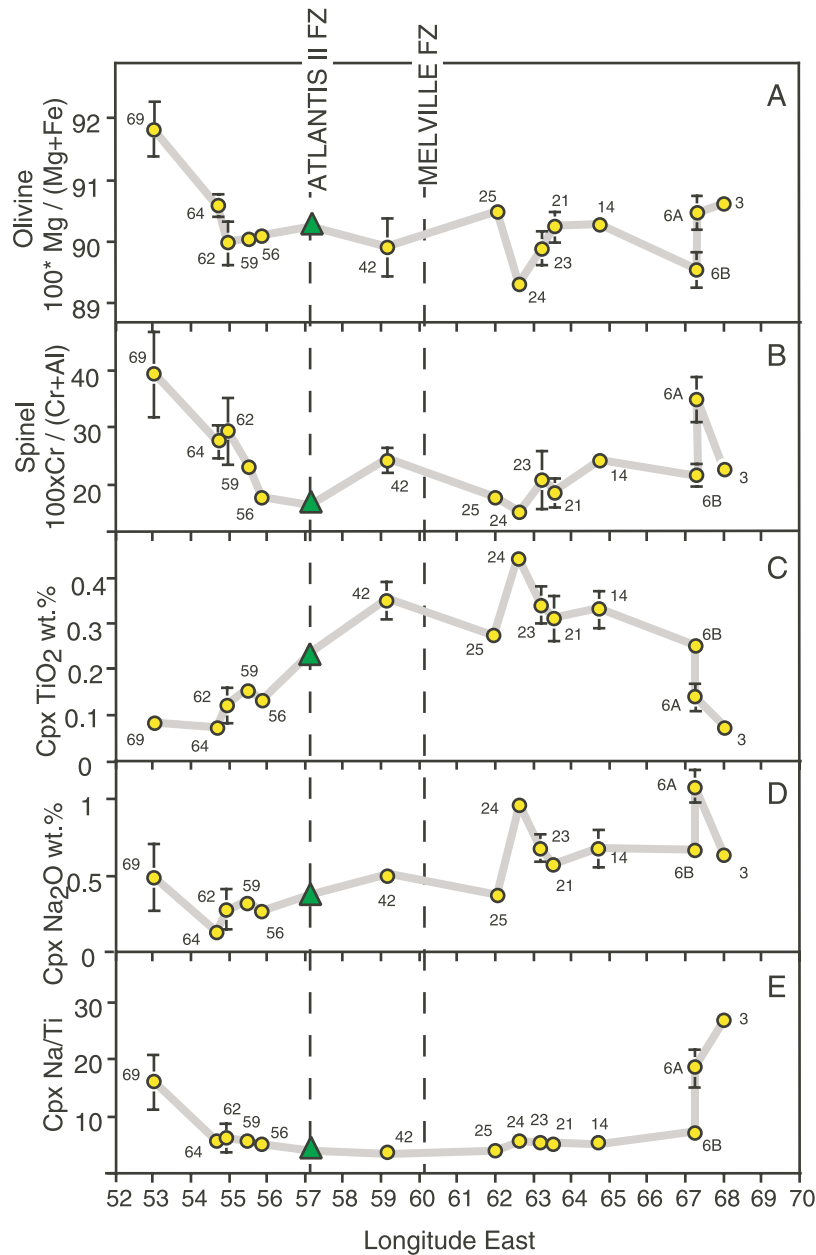


Figure 12. Along-axis variations of the olivine, spinel and clinopyroxene compositions of EDUL peridotite samples (averages and standard deviation per dredge) between 52°E and 68°E. The composition of the Atlantis II Fracture Zone peridotite is from *Johnson and Dick [1992]*.

tents in the average of the EDUL suite, but anomalously high Na/Ti ratios result from very low TiO₂ contents.

4.3. Modal and Whole Rock Variability

[32] Table 2 suggests an overall trend to more harzburgitic peridotites as going from east to west, and also shows that the peridotites to the east of

Melville FZ are more heterogeneous than the peridotites to the west of Melville. In particular, true lherzolites (cpx ≥ 6%) are observed only to the east of Melville, and they are associated with harzburgites very depleted in cpx (Figure 3). Furthermore, in two eastern dredges (21 and 23), the distribution of the mineral phases varies largely among samples from the same dredge, although there is no correlation between mineral proportion

Table 7. Reconstructed Mantle Mineral Phase Proportions (vol.%) and Bulk Chemical Compositions (wt.%) for Four Selected Dredges (3, 21, 62 and 64)^a

Dredge #	3	21	21	21	62	69
Lithology	harzburgite	lherzolite	harzburgite	lherz/harzb	lherz/harzb	harzburgites
Number of samples	1	1	1	4	4	6
Number of points	10566	10416	11144	37560	28468	30192
<i>Mineral vol.%</i>						
Olivine	71.0	68.7	70.3	68.9	72.3	68.5
Orthopyroxene	24.0	22.7	27.3	25.4	23.0	29.5
Clinopyroxene	3.8	7.3	2.1	4.7	3.6	1.1
Spinel	0.6	1.3	0.3	1.0	1.1	0.9
<i>Oxide wt.%</i>						
SiO ₂	43.94	43.86	44.45	44.11	43.60	44.72
TiO ₂	0.01	0.05	0.03	0.04	0.02	0.01
Al ₂ O ₃	1.60	2.45	1.74	2.23	1.73	1.50
Cr ₂ O ₃	0.43	0.55	0.30	0.47	0.62	0.69
FeO	8.19	8.30	8.43	8.36	8.53	7.08
MnO	0.13	0.12	0.12	0.12	0.13	0.14
MgO	43.89	42.20	43.47	42.70	43.90	44.69
NiO	0.34	0.27	0.27	0.27	0.30	0.30
CaO	1.43	2.15	1.15	1.66	1.16	0.84
Na ₂ O	0.05	0.06	0.04	0.05	0.01	0.02

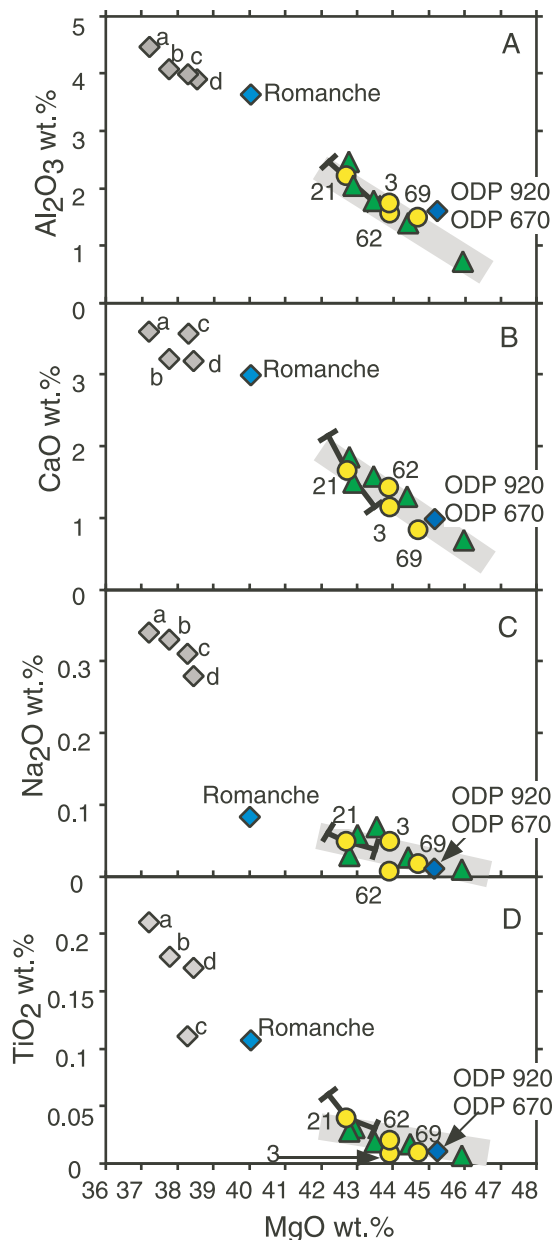
^a Modal compositions were established by point counting at 0.5 mm spacing. Number of samples and number of point counts per dredge are given.

and mineral composition. In dredge 21, we observe a normal distribution around a mean of about 5 vol.% cpx (4 samples); 2 samples are true harzburgites with a minimum cpx content of ~2%, and 2 samples are true lherzolites with a maximum cpx content of ~7%. In dredge 23, the cpx content in the 4 studied samples ranges from almost 0 to 8 vol.%, with a mean content of ~4%. To the west of Melville, the dredges display homogeneous intrasample and intradredge modal compositions. Between Melville and Atlantis II FZ, the upper-mantle appears dominantly harzburgitic (dredge 42). Between Atlantis II and Gauss FZ (dredges 56–64), samples define an average lherzolitic/harzburgitic upper mantle with ~4–<6 vol.% cpx, like to the east of Melville, but with a more restricted range of compositions. Finally, between Gazelle and Galieni FZ, dredge 69 consists of homogeneous, cpx-poor, opx-rich harzburgites; they have the most refractory composition of the studied EDUL area. These observations, however, are limited by the uneven representation of each dredges. Among all the dredges, only seven (dredges 21, 23, 25, 56, 62, 64, 69) contain enough material

(>200 kg) to constrain the modal composition and variability of the local upper mantle.

[33] Modal compositions of 15 samples representing 4 dredges are presented in Table 7. Each sample has been cut in 1cm-thick slices, and the surfaces (48 to 108 cm²-sized) observed for intrasample modal variability. Rough visual estimates show that the proportions of the olivine/opx/cpx grains (size >5 mm) are homogeneous throughout individual samples at this scale. Then, a slice of each sample was cut in standard-sized thin sections, and more precise modal proportions was established by point counting. Each sample modal analysis represents between 10,000 to 12,000 point counts at 0.5 mm spacing. Data represent the original mineral proportions (“primary” modes) established in counting pseudomorphs with relict mineral phases, and are not corrected for differential volume expansion during serpentinization. Bulk compositions (Table 7) have been calculated using average mineral compositions for each sample or group of samples and average modal data converted to weight fraction (in the case of dredge 69, in the absence of

preserved olivine, olivine Mg# was inferred from the Mg# of opx, using a partition coefficient of 0.998). Three calculations have been performed for dredge 21, corresponding to the average of four lherzolitic/harzburgitic samples and to the cpx-rich and cpx-poor end-members. Since there is no systematic relation between cpx proportion and composition of mineral phases, this detailed analysis allows us to evaluate the uncertainty on the whole rock composition caused by varying mineral proportions.



[34] In oxides versus MgO wt% diagrams (Figure 13) EDUL compositions plot on the abyssal peridotite array defined by the least and the most depleted Mid-Atlantic Ridge peridotites of *Michael and Bonatti* [1985], and by other SWIR and American - Antarctic Ridge peridotites [*Dick*, 1989; *Johnson and Dick*, 1992], including those from Bouvet FZ known as the most depleted abyssal peridotites, and from Atlantis II FZ/ridge intersection [*Dick*, 1989; *Johnson et al.*, 1990].

[35] EDUL samples display a wide range of variation along this array, but are significantly more depleted than the Romanche FZ spinel-peridotites [*Bonatti et al.*, 1993]. The more depleted peridotites (dredge 69) are close to the MARK peridotites in this diagram, but their modal compositions and mineral chemistry are quite different. Dredge 69 harzburgites are poorer in olivine but richer in opx (69 and 29 vol.%, respectively) than harzburgites from ODP sites 670 and 920 (76–79% olivine and 16–19 vol.% opx [*Komor et al.*, 1990; *Stephens*, 1997]).

[36] Between 62° and 65°E, the samples display the largest modal variability, although mineral compositions remain relatively homogeneous. To get an estimate for the average composition of the local mantle, we have calculated the bulk composition of the 22 samples collected from this area.

Figure 13. (opposite) MgO versus Al₂O₃, CaO, Na₂O and TiO₂ (wt.%) in reconstructed bulk compositions of four EDUL dredges (3, 21, 62 and 69; yellow dots). The error bars for dredge 21 correspond to inhomogeneous distribution of clinopyroxene in the peridotite set. For comparison, following compositions are plotted: Mantle source compositions: (a) primitive mantle of *Sun and McDonough* [1989] and (b) of *Hart and Zindler* [1986]; (c) experimental depleted lherzolite MM-3 of *Baker and Stolper* [1994]; (d) depleted MORB mantle of *Hart and Zindler* [1986]. Other abyssal peridotites from the Atlantic ocean: spinel-lherzolites from the Romanche Fracture Zone [*Bonatti et al.*, 1993]; peridotites from ODP sites 670 and 920 [*Komor et al.*, 1990; *Stephens*, 1997]; Mid-Atlantic peridotite compositional array of *Michael and Bonatti* [1985] (gray thick line). Other SWIR peridotite compositions (green triangles), by increasing MgO wt.%, peridotites from Vulcan, Atlantis II, Islas Orcadas, Bullard and Bouvet Fractures Zones [*Dick*, 1989; *Johnson and Dick*, 1992].

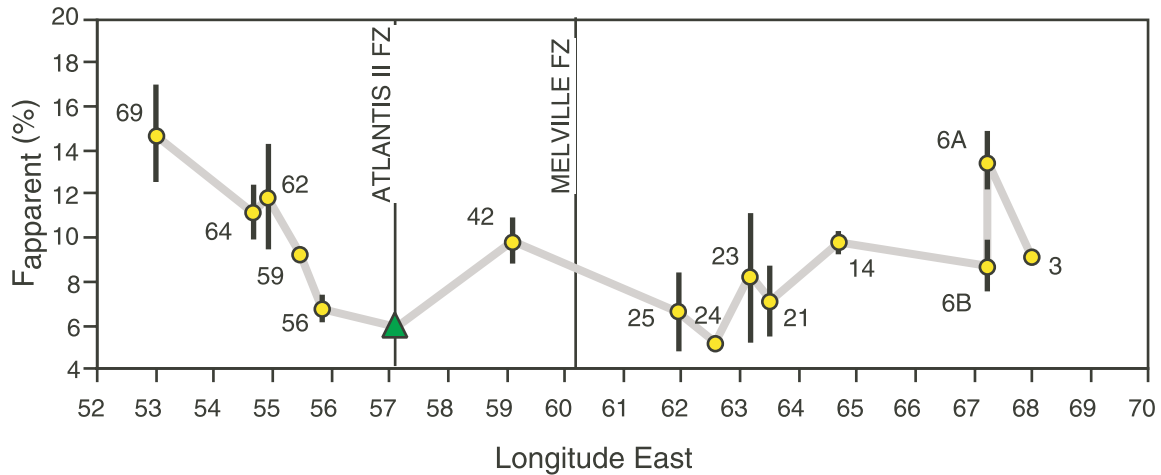


Figure 14. Along-axis apparent melting degrees of EDUL peridotites (averages and standard deviations per dredge) calculated from Cr/(Cr + Al) ratio in spinels using the relation of *Hellebrand et al.* [2001]. The composition of the Atlantis II Fracture Zone peridotite is from *Johnson and Dick* [1992].

We use the phase proportions given by Tables 2 and 7 (6 vol% cpx and olivine/opx ratio = 2.7) and the average compositions of the porphyroclast cores (Tables 3–6). The calculated SiO₂ (44.1 wt%), MgO (42.2 wt%), Al₂O₃ (2.6 wt%), TiO₂ (0.05 wt%) and Na₂O (0.05 wt%) concentrations are in the average of the less depleted abyssal peridotite compositions compiled by *Niu* [1997]. The calculated CaO content (1.7 wt%) is also in the range of abyssal peridotites, although plotting at the extreme lower bound in the CaO versus MgO compositional trend of *Niu* [1997]. This calculated composition (Na₂O and CaO excepted) corresponds to about 12–13% fractional melting of DMM compositions in the models of *Niu* [1997] and *Kinzler and Grove* [1992b]. The fertile EDUL mantle thus appears to be slightly impoverished in cpx component with respect to an overall ~12–13% melting residual composition of typical MORB mantle source composition.

5. Degree of Melting of Edul Peridotites

[37] The degree of melting of abyssal peridotites can be estimated using the Cr# of spinels, assuming that residual mineral compositions are preserved. Because of the inconsistencies that we have pointed out in associated mineral compositions, the significance of this estimation can be questioned. Nevertheless, we have tried to quantify

the apparent extent of melting (F) in the EDUL sample set with the empirical equation [$F = 10 \ln(\text{Cr}\#) + 24$] proposed by *Hellebrand et al.* [2001] (Figure 14). The most aluminous samples belong to dredges 21–25 in the 61–64°E region, and correspond to ~5% melting. The most depleted sample belongs to dredge 69, and corresponds to ~17% melting (Figure 14). This is similar to the melting range calculated by *Hellebrand et al.* [2001] for abyssal peridotites from the MARK area in the Atlantic ocean. Calculated F values show a general decrease from the RTJ (70°E) to the 62–64°E region (dredge 24) although two very different values coexist in dredge 6. To the west of Atlantis II FZ, calculated F increase westward, starting from values as very low as those calculated in the 62–64° E region (Figure 14). Dredge 42 value, between Melville and Atlantis II FZ, appears anomalously high with respect to the adjacent calculated F values.

[38] Another melting indicator is provided by cpx Ti content which decreases in abyssal peridotites with increasing degree of melting, provided the residual rock has not been subjected to secondary Ti enrichment and that subsolidus exchange reactions did not modify the mineral equilibria. Modeling of *Johnson et al.* [1990] shows that after small degrees ($\leq 12\%$) of fractional melting of a depleted lherzolitic source, residual cpx and bulk

residue are still relatively rich in Ti (≥ 0.3 wt% and ≥ 0.06 wt% TiO₂, respectively). Similar high TiO₂ contents are observed in the cpx of peridotites dredged between 65 and 59°E (dredges 14–42). The highest concentrations are found in the sample from dredge 24, and corresponds to $\sim 6\%$ fractional melting in *Johnson et al.*'s [1990] model. East and west of this fertile mantle section, TiO₂ contents in cpx decrease, corresponding to 17 and 24% fractional melting in samples 6A and dredge 3, respectively, and to 20–24% fractional melting in dredges 62–69. There is a relatively good correlation between melting estimates calculated with Cr# in spinel and with TiO₂ in cpx for fertile samples. In contrast, in refractory samples, melting degrees estimated with TiO₂ in cpx are significantly greater than those calculated with Cr# in spinel. However, when whole rock TiO₂ concentrations are calculated using opx and cpx proportions and compositions, samples from dredges 3, 62 and 69 are less refractory than suggested by TiO₂ contents in the only cpx, although dredges 3 and 69 still plot slightly below the abyssal peridotite trend in the TiO₂ versus MgO diagram (Figure 13). Similar conclusion, that opx does take in a greater proportion of the whole rock Ti as melt depletion increases, was reached for other peridotite suites by *Rampone et al.* [1991] and *McDonough et al.* [1992]. This suggests that, in the most refractory peridotites, a high proportion of bulk TiO₂ resides in the opx.

6. Discussion

6.1. Major Compositional Features of the EDUL Peridotites

[39] At a broad scale, compositional variations in the EDUL peridotite sample set are characterized by increases in the Mg# of silicates and in the Cr# of spinel and pyroxenes, whereas Al₂O₃ and TiO₂ contents in opx and cpx decrease. Bulk-rock major element compositions established for representative dredges plot on the abyssal peridotite array, characterized by inverse correlation of Al₂O₃, CaO, TiO₂ and Na₂O with MgO. Dredges that contain mostly lherzolites have minerals more enriched in basaltic components (Fe, Al, Ti) and

dredges that contain mostly harzburgites have minerals more enriched in refractory elements (Mg, Cr). All these data suggest that the EDUL peridotites represent residual mantle, subjected to variable degrees of depletion by partial melting and extraction of basaltic melt. Apparent extents of melting based on spinel Cr# range from ~ 5 to $\sim 17\%$ as for MARK peridotites in the Atlantic ocean. However, major inconsistencies occur when small scale variations in mineral compositions, pyroxene Na₂O contents and bulk rock compositions are considered.

[40] At a small scale, chemical parameters that are known to be very good tracers of the partial melting, such as Cr# in spinel and pyroxenes, Mg# in silicates and TiO₂ contents in cpx, are frequently poorly correlated, resulting in meso-scale heterogeneities. In other words, for a given sample, the apparent degree of partial melting varies depending on the selected indicator. Sub-solidus reequilibration to lower pressure and temperature conditions and late-stage melt-rock interaction may modify mineral compositions. We infer that such reequilibration is responsible for chemical zoning in pyroxenes (Figures 5 and 7). However, in discarding plagioclase-bearing samples and in restricting our sample set to peridotites containing low-Ti spinels, we are confident that these modifications should have been modest. Thus, we suggest that heterogeneity and discrepancy in mineral compositions should be discussed in terms of early melt-rock interaction and/or initial heterogeneity.

[41] If the extent of melting inferred from spinel Cr# and pyroxene Ti contents are similar to those measured in the MARK area, the sodium content of EDUL and MARK cpx are totally different. EDUL cpx are in the whole enriched in jadeite component (e.g., characterized by higher Na₂O content and higher Al^{VI}/Al^{IV} ratio) relative to MARK cpx (Figure 10). The most fertile EDUL peridotite (dredges 21 to 25) cpx contain 0.53–1.3 wt% Na₂O, twice more than the equivalent from Kane FZ cpx (0.27–0.53 wt% [*Ghose et al.*, 1996]) for similar calculated extents of melting. EDUL values can be compared to those observed

in the Romanche FZ [Seyler and Bonatti, 1997]. But the latter display all the characters of fertile peridotites (very low spinel Cr#, low olivine and opx Mg#, high modal cpx). In contrast, EDUL peridotites have clearly undergone higher degrees of melting, yet their cpx have similar to higher Na₂O contents. This striking feature is inconsistent with these peridotites being simple melting residues of a homogeneous MORB source composition: the very low degree of melting suggested by such high Na₂O concentrations seems incompatible with their Al contents and their Mg# and Cr# which are in the average of other abyssal peridotite minerals (Figures 10a and 11). Furthermore, dredges most enriched in refractory components and most depleted in basaltic components (dredges 3, 6, composition A, and 69) display anomalously Na₂O-rich cpx and opx (Figures 6d, 8d, and 12d).

[42] Finally, although reconstructed whole rock compositions are consistent with the calculated extents of melting (Figure 13), they are in contradiction with the overall low proportions of modal cpx. In the 22 samples collected from the 62–65°E area, melting degrees estimated from Cr# in spinel and TiO₂ in cpx range from 5 to 11% (average 8%) and from 7 to 12% (average 10%), respectively. Such low degrees of melting of an average depleted MORB mantle (DMM) source containing 17–20% cpx leave a residual solid with 8–12% cpx [Johnson *et al.*, 1990; Kinzler, 1997; Niu, 1997]. Yet, the average percentage of cpx in the samples lies between 5–6% cpx (Table 2), with a maximum of 8%, much lower than the predicted values. In addition (as important as the average depletion in cpx), modal compositions are highly variable at small scale, and there is a lack of correlation between mineral proportion and compositions: almost half of dredge 21 and 23 samples are harzburgites, some very depleted in cpx (Table 2) although they have fertile mineral compositions. Harzburgites from dredge 69 are also anomalously rich in opx, relative to olivine (Figure 13), and have anomalously high silicate Mg# (Figures 6b, 8b, and 11).

[43] In summary, EDUL peridotites display three major characteristics: strong local and regional

mineral heterogeneities, pyroxenes enriched in jadeite component and overall low abundance of cpx. Furthermore, apparent degree of melting is higher than predicted by the morphology of the ridge and the compositions of the associated basalts. Various processes may explain the particular features of these peridotites, including the tectonic setting, metasomatic reactions with melts and heterogeneous mantle source. These possible scenarios are addressed in the following sections, but our preference goes to a heterogeneous mantle source.

6.2. Influence of the Tectonic Setting

[44] The samples have been systematically dredged in similar tectonic setting, i.e., at segment discontinuities, where the higher mantle Bouguer anomaly indicates a thinner crust, except for dredges 23 and 69. Figure 14 could suggest that the two major transform faults, Atlantis II and Melville, have an influence on the degree of melting which seems to be lower in their vicinity. However, the distance between the dredges and the transform faults always remain very large. For instance, dredge 56, the closest, is located more than 100 km away from Atlantis II FZ. For comparison, in the MARK area, the transform fault effect has already disappeared in samples located only 30 km away from the Kane FZ [Ghose *et al.*, 1996]. Moreover, the western portion of the studied area is shifted by three smaller transform faults (Gauss, Gazelle, Gallieni; see Figure 2) which obviously have no effect on the extent of melting.

[45] East of the Melville FZ, there is a small overall decrease of the extent of melting westward, but the distance to the fracture zone is very large. The closest dredge, dredge 25, is located more than 200 km away. Although there are no transform fault east of Melville, the peridotites from this area are the most heterogeneous. Therefore we consider that the along-axis variations cannot be attributed to transform fault effects.

6.3. Refertilization of the SWIR Lithospheric Mantle

[46] EDUL cpx compositions may have been modified by interaction with magmas migrating

upward through the subaxial lithospheric mantle. We used the associated basalt compositions to test whether interactions with basaltic melts could explain the high Na₂O contents of the peridotite cpx. Compositions of cpx and spinel in equilibrium with the SWIR basalts have been calculated using partition coefficients obtained from experimental runs [Kinzler and Grove, 1992a; Kinzler, 1997; Falloon *et al.*, 1997, 1999; Robinson *et al.*, 1998; Pickering-Witter and Johnston, 2000] in which lherzolitic assemblages are in equilibrium with melts of same compositions as the SWIR parental magmas (e.g., glasses corrected for low pressure crystal fractionation [Humler *et al.*, 1998]). Results show that re-equilibration of the peridotites with the bulk compositions of the EDUL basalts, in the 1.0–1.5 Gpa pressure range, could explain the high Na₂O contents of most EDUL cpx, in particular those from dredges 3, 6, composition A, and 69, but fails to account for the low TiO₂ contents of these cpx and for the very low TiO₂ contents of the associated spinels. This conclusion is supported by the compositions of the interstitial cpx from dunites dredged with the peridotites, which are thought to represent fossil melt channels. In contrast with peridotite cpx, these cpx, as well the associated Cr-spinels, are enriched in TiO₂ (0.4–0.8 and ≥ 0.3 wt% TiO₂, respectively).

[47] A second possible mechanism is enrichment of the cpx by diffusive infiltration of Na from early, alkali-rich, high-pressure partial melts into the shallower, partially molten peridotite [Lundstrom, 2000]. According to Lundstrom [2000], this process significantly increases Na₂O, but not TiO₂, in the solid. This process could have been active in EDUL cpx that show Na enrichment relative to Ti. Similarly, Na₂O-rich cpx inclusions, with up to 1.4 wt% Na₂O, that occur in several samples could have been in equilibrium with highly alkalic melt (Na₂O > 5%), e.g., silica-rich melt from incipient melting of a fertile mantle source [Baker *et al.*, 1995; Robinson *et al.*, 1998]. However, in some EDUL cpx, and particularly in cpx from dredges 3, 6, composition A, and 69, the very high Na/Ti ratios are also caused by strong depletion in Ti. This rather suggests that major depletion in peri-

dotite and metasomatizing melt belong to two separate events.

[48] A third scenario is that EDUL residual mantle was modally modified with respect to theoretical residual mantle by melt impregnation and crystallization, as suggested by the inhomogeneous distribution of the cpx at a small (intradredge) scale, with coexistence of lherzolitic and harzburgitic samples, some of the latter being almost totally cpx free. Furthermore, the near cpx-free harzburgites are not impoverished in opx, e.g., are still characterized by low olivine/opx ratios similar to those characterizing the lherzolites, and, in the lherzolites, cpx tends to occur in groups of crystals with texture suggestive of magmatic crystallization (section 3). Refertilization by incremental, or not fully aggregated, melts produced during fractional melting may have occurred at high temperature, at the base of a deep subaxial lithosphere. This hypothesis is supported by the fact that the large crystals of cpx are in textural equilibrium within the coarse-grained mineral assemblages; they underwent high-temperature, plastic deformation responsible for their occurrence as porphyroclasts. The enrichment in Na is not only observed in the cpx porphyroclasts, but also affects the cores of the largest opx grains and not the rims (Figure 5). All these data indicate that, if cpx did crystallize from melt, this crystallization took place before high-temperature annealing in the spinel stability field, prior to lithospheric cooling. However, these cpx also occur as ragged crystals with spongy rims (Figure 4d), that suggests that they were partially molten during the ductile deformation, and, thus, already present in the protolithic mantle. Depletion in cpx by partial melting and refertilization by melt impregnation might have also occurred before the SWIR decompressional event. Additional evidence for very early melt-rock interaction is the presence, in most samples, of inclusions of cpx in large opx grains, often associated with olivine and spinel and occasionally associated with hydrous mineral phases [Seyler *et al.*, 2002]. Some of these inclusions may have crystallized from melt (as suggested by occasional magmatic twins in cpx), either resulting from partial melting of the opx hosts or from melt that penetrated within them. The

mineralogy of these inclusions (cpx \pm olivine \pm spinel), and their frequent coarse and euhedral shapes are indicative of high-temperature annealing in the spinel stability field. Cpx inclusions display a large range of compositions in individual samples (Figure 6), but are generally more fertile in terms of Na and Ti contents than granular cpx in the same sample. The highest Na and Ti contents for cpx of the EDUL sample set are found in inclusions in a harzburgite devoid of matrix cpx (sample 23-2-1). Matrix cpx in other samples from the same dredge are significantly poorer in Na and Ti. Spinel inclusions in opx have been found in two samples from dredges 23 and 62 (samples 23-2-1 and 62-4-3) and are more aluminous than spinels in the granular assemblage of their host samples. These inclusions are therefore in compositional disequilibrium with the minerals of their host rock. Our proposed interpretation is that they represent relict minerals, preserved within large opx grains, and bear witness of very early impregnation by melt. Work is underway to detail the microstructural and chemical properties of these inclusions and their petrological implications [Seyler *et al.*, 2002; Seyler, manuscript in preparation, 2002].

6.4. Models for a Modified Mantle Source

[49] The last possible scenario is that the high Na content of the cpx, together with the overall low abundance of this mineral phase in EDUL samples, may have been inherited from the initial pyroxenes of the peridotitic mantle, which was characterized by bulk Na/Ca content higher than in common MORB mantle source. Such characteristic may result from refertilization of a previously depleted mantle. The calculated global composition of the mantle beneath the 62–65°E region has shown a slight depletion in CaO with respect to other oxide residual composition. If the initial composition was lower in modal cpx at normal bulk Na concentration, this may explain the high Na content in the residual cpx.

[50] With the exception of dredges 3, 6, composition A, and 69 and two samples in dredge 62, EDUL peridotite cpx (and opx; Figure 8d) have Na₂O contents negatively correlated with Cr#

(Figure 6d) and positively correlated with TiO₂ contents, and plot in or near experimental melting compositions in a Na₂O-TiO₂ diagram (Figure 15). This suggests that the compositions of these cpx may be controlled by partial melting of a peridotite source. The experimental fields in Figure 15 are defined by compositions of residual cpx after variable degrees of melting of various bulk mantle compositions at 1 and 1.5 GPa [Baker and Stolper, 1994; Robinson *et al.*, 1998; Falloon *et al.*, 1999; Pickering-Witter and Johnston, 2000; Schwab and Johnston, 2001]. Dredge 14, 21, 23 and 42 cpx plot close to experimental cpx, corresponding to \sim 5% melting of DMM-like compositions at 1 GPa; these compositions could also be residues of higher extent of melting at 1.5 GPa. Dredge 24 cpx have more fertile compositions, close to experimental cpx of \sim 5% melting at 1.5 GPa. Dredge 56–64 cpx have compositions corresponding to higher degrees of melting of similar sources, or to low degrees of melting of more depleted source compositions. Because mantle melting beneath oceanic ridges is near-fractional, not batch melting, we compared models of residual cpx compositions calculated from fractional melting equations of Johnson *et al.* [1990]. Melting reactions and Na and Ti partition coefficients are taken as a function of pressure [Kinzler and Grove, 1992a; Kinzler, 1997, Table 8]. Our results show the following. (1) The slope of EDUL cpx compositional trend can be reproduced by isobaric fractional melting (although for pressures \geq 1.8 GPa in order to retain high Na₂O contents in the cpx) but cannot be reproduced by any polybaric fractional melting models. Polybaric fractional slopes are steeper than isobaric melting slopes because, as pressure decreases, Na₂O partitioning between pyroxenes and melt decreases, whereas TiO₂ partitioning tends to increase [Blundy *et al.*, 1995; Putirka, 1999; Kinzler and Grove, 1992a, 1992b; Kinzler, 1997] (TiO₂ partitioning also decreases as Al₂O₃ decreases in cpx and melt with increasing degree of melting [Baker *et al.*, 1995; Putirka, 1999]; for the purposes of the melting model presented here, TiO₂ partitioning was considered as constant). (2) Most of the compositions of the cpx from dredges 14–42 plot along a calculated polybaric (2.0–0.8 GPa) frac-

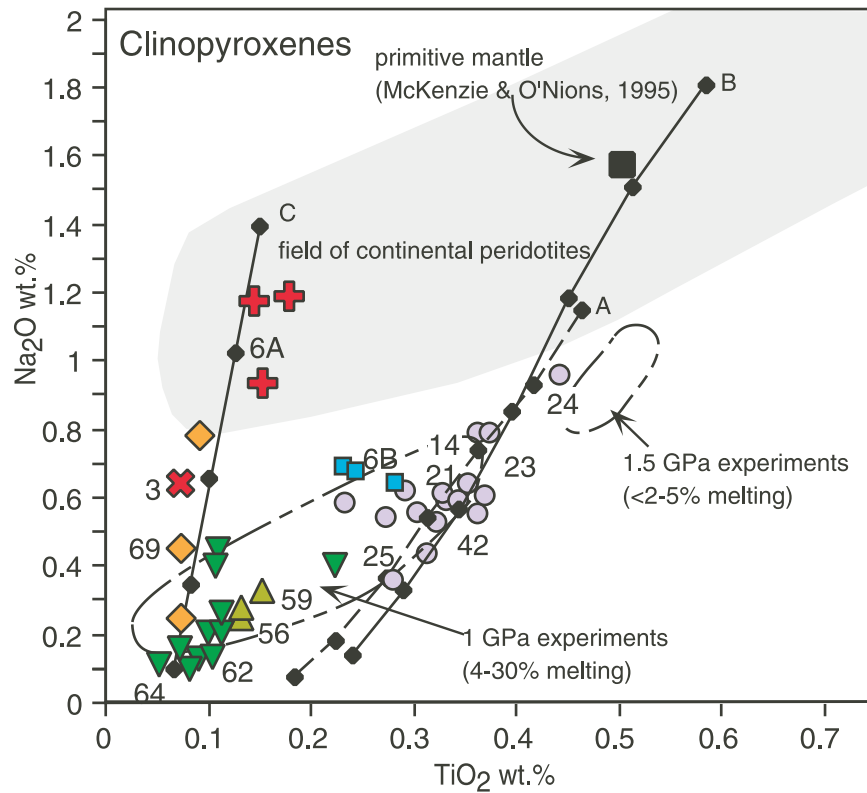


Figure 15. Na₂O versus TiO₂ (wt.%) in EDUL clinopyroxenes (averages of porphyroclast cores per sample): red crosses indicate dredges 3 and 6, composition A; blue squares indicate dredge 6, composition B; purple circles indicate dredges 14 to 42; green triangles indicate dredges 56 and 59; green inverted triangles indicate dredges 62 and 64; orange diamonds indicate dredge 69. Fields of experimental cpx from *Baker and Stolper* [1994], *Robinson et al.* [1998], *Falloon et al.* [1999], *Pickering-Witter and Johnston* [2000], *Schwab and Johnston* [2001]. Field of continental lithospheric mantle clinopyroxenes according to *Seyler and Bonatti* [1994]. Primitive mantle clinopyroxene of *McKenzie and O'Nions* [1995]. Curve A, polybaric fractional melting of a depleted MORB mantle source clinopyroxene. Curve B, polybaric fractional melting of a clinopyroxene from a source enriched in Na and Ti. Curve C, polybaric fractional melting of a clinopyroxene from a source modified by melt extraction and possible metasomatism. Initial mode for curves A and B are from *Hart and Zindler* [1986]. Initial Na₂O and TiO₂ compositions for curve A are from *Hart and Zindler* [1986]. Initial Na₂O and TiO₂ compositions for curve B, and initial mode and initial Na₂O and TiO₂ compositions for curve C were chosen in order to fit EDUL compositions (see text); these values are within the range of fertile and depleted natural peridotites [*Seyler and Bonatti*, 1994]. Melting reactions and partition coefficients for Na₂O between pyroxenes/liquid vary with pressure; values are calculated in regressing the lines defined by the higher and lower pressure experimental values of *Kinzler and Grove* [1992a], *Kinzler* [1997], *Falloon et al.* [1997, 1999] and *Robinson et al.* [1998] (see Table 8). Melting begins at 2 GPa and the mantle is assumed to melt 1%/kbar. Ticks = 2% melting.

tional melting curve for a DMM composition (curve A in Figure 15). However, to reconcile the high Na₂O contents in the cpx with the ~5–11% melting range calculated with the spinel Cr#, the composition of the mantle source must be richer in Na₂O and TiO₂ than the DMM composition for similar mineral proportions (curve B in Figure 15). The initial composition required (bulk Na₂O = 0.46 wt%; bulk TiO₂ = 0.22 wt%) is however in the range of primitive mantle compo-

sitions [*Falloon and Green*, 1987; *Hirose and Kushiro*, 1993; *McDonough and Sun*, 1995]. The required initial cpx must be enriched in Na and Ti with respect to cpx in the primitive mantle of *McKenzie and O'Nions* [1995] and plots in the Na₂O-TiO₂ field of cpx from fertile peridotites. These fertile peridotites are those used to establish primitive mantle compositions [*Jagoutz et al.*, 1979; *McDonough and Sun*, 1995]. (3) In this model, dredge 56–64 cpx could be residues of

Table 8. Starting Compositions and Na₂O and TiO₂ Partition Coefficients Between Mineral/Liquid Used to Calculate the Three Model Curves Plotted in Figure 15 (see Text and Figure 15 for Data Source)

	Initial mode Curves A and B	Initial mode Curve C	Melt mode at 2 GPa	Melt mode at 1.2 GPa
Olivine	0.54	0.67	-0.14	-0.30
Orthopyroxene	0.23	0.20	-0.05	0.25
Clinopyroxene	0.20	0.10	1.08	0.97
Spinel	0.03	0.03	0.11	0.08
Initial oxide concentrations (wt.%)				
	Na ₂ O Bulk	Na ₂ O Clinopyroxene	TiO ₂ Bulk	TiO ₂ Clinopyroxene
Curve A	0.28	1.10	0.174	0.46
Curve B	0.46	1.80	0.22	0.58
Curve C	0.21	1.41	0.04	0.15
Mineral/liquid partition coefficients				
	Na ₂ O at 2 Gpa		Na ₂ O at 1 Gpa	TiO ₂
Olivine	0.001		0.001	0.02
Orthopyroxene	0.07		0.03	0.17
Clinopyroxene	0.30		0.14	0.30
Spinel	0.001		0.001	0.12

higher melting extents of an initial cpx that is poorer in TiO₂.

[51] Cpx from dredges 3 and 6, composition A, from most samples in dredge 69 and from two samples in dredge 62 plot at high Na₂O and very low Ti₂O contents (Figure 15). Several mechanisms can be inferred to explain these particular compositions. A possible interpretation can be that the cpx from the protoliths were low in TiO₂ with respect to Na₂O, similar to the composition in some peridotites from continental environments (Figure 15). This fractionation of Na relative to Ti in cpx may have resulted, as commonly proposed for within-plate residual peridotites, either from partial melting at very high pressure [Putirka, 1999], generating residual pyroxenes with high Na/Ti, or from contamination of residual mantle by small-melt volumes characterized by high Na/Ti, followed by equilibration in the spinel lherzolite facies. In this interpretation, these events would have occurred in the mantle before upwelling and partial melting beneath the SWIR. Curve C (Figure 15), starting from an initial composition more depleted than for curve B (Table 8), suggests that very small amounts of decompression melting beneath the SWIR could account for the dispersion of dredges 3, 6, composition A, and 69 samples,

samples from dredge 3 having undergone more melting than samples 6A.

6.5. Evidence for Along-Axis Heterogeneous Mantle Source Composition

[52] The general decrease in average axial depth from east to west is interpreted in terms of increasing degree of melting [Cannat *et al.*, 1999]. This general trend is somehow confirmed by the basaltic glass Na_{8.0} content which tends to decrease from east to west [Humler *et al.*, 1998]. The basalt compositions, however, display some scattering and are not so consistent if other parameters are considered. In particular, they are consistently depleted in Ti east of the Melville FZ, and this particular feature is inferred to result from source effect [Meyzen *et al.*, 2003].

[53] If the peridotites are considered, some discrepancies arise. Figure 12d shows a general decrease in the Na₂O contents of cpx which broadly correlates with along-axis variation of Na_{8.0} in basalts. However, we have pointed out that Na₂O contents of cpx are often in contradiction with other indicators of melting. The highest Na/Ti contents in cpx occur in peridotites from the easternmost area (dredges 3 and 6 composition A), where cpx are also very depleted

in Ti but very enriched in Cr, and where the Cr# of spinel increases. These refractory compositions suggest high degrees of melting which are not consistent in this context of very slow/cold ridge nor with the basalt Na8.0 which indicates very low degree of melting. Therefore we propose that the refractory mineral compositions pre-dated the last melting event related to the opening of the SWIR. Whatever the cause of the pyroxene Na₂O enrichment, only very low degree of melting can have preserved it. The upper mantle in this 67–68°E region is especially heterogeneous (mineral chemistry of dredge 6 samples is bimodal) and show evidence for ductile shearing (dredge 6 is the only dredge to contain mylonites), that suggests that this region may act as a compositional/tectonic boundary.

[54] From 67°E to Melville FZ, inconsistencies and heterogeneities are obvious when modal and mineral compositions are considered. Harzburgites are abundant in the most fertile region (62–65°E, dredges 21 to 25) defined by the Cr# in spinels. These cpx-poor samples have nevertheless mineral compositions as fertile as in lherzolites and are equilibrated at the same pressure-temperature conditions. It should also be noted that extreme modal heterogeneity occurs in the region where calculated melting degrees are quite variable at a local scale (Figure 14). These extreme compositional heterogeneities coincide with extreme rugosity of the axial relief and maximum axial depth, and with the more peculiar compositions of the basalts [Meyzen *et al.*, 2002, 2003]. In this portion of the SWIR, the compositional features of the peridotites are certainly in relation with very slow spreading and extremely low degrees of melting. In this environment, initial heterogeneity of the mantle source may have a considerable influence on the melting regime, resulting in enhanced compositional variations in the subaxial mantle at small and regional scales.

[55] West of Atlantis II FZ, the peridotite compositional heterogeneities are less marked, and the modes of the peridotites are much more homogeneous at a dredge scale. Axial valleys in this region are also shallower and less irregular, and the basalts display more “normal” compositions, although the average extent of melting is still expected to be

lower than in other mid-ocean ridge regions. In the 54°–56°E region, Cr# in spinel and TiO₂ contents in cpx suggest increasing degrees of mantle melting from dredge 56 to dredge 64. This increase in the extent of melting is not observed in basalt compositions [Meyzen *et al.*, 2002, 2003], and dredges 56 and 59 have compositions inconsistent with the degree of melting predicted from the axial depths [Cannat *et al.*, 1999]. Furthermore, the compositions of the pyroxenes change abruptly from the Melville region (including dredge 42) to Atlantis II FZ (marked by the lowering of TiO₂ and Na₂O in dredge 56 and 59 opx and cpx, for similar Cr#; Figures 6, 8, and 12), suggesting that this fracture zone seems to form a major compositional discontinuity. Cpx Na₂O-TiO₂ modeling (Figure 15) indeed supports this hypothesis: peridotite compositions of these dredges located west of Atlantis II may be explained by low to moderate degrees of melting of a source different from that of dredges 42 to 14, located east of Atlantis II.

[56] Cpx from dredge 69 peridotites are chemically heterogeneous and also highly enriched in Na with respect to Ti, Mg# and Cr#. In this region, the axial depth is higher than in the 54°–56° E region (Figure 2), and the basalts again show high Na_{8.0} and geochemical anomalies [Meyzen *et al.*, 2002, 2003]; the upper mantle was thus expected to be less depleted than to the west of Gauss FZ. Hence, these peridotites have the more refractory compositions of the studied area, and stand apart the other EDUL peridotites in terms of mineral and modal compositions. They actually share several characteristics with harzburgites that occur as xenoliths in the South African kimberlites, such as low olivine/opx ratios and very high silicates Mg# with respect to spinel Cr# and to olivine abundance [Boyd, 1989; Kelemen *et al.*, 1998]. These very special compositions further strengthen the hypothesis of major compositional heterogeneity of the protolithic mantle in this region of the SWIR sampled during EDUL cruise.

7. Summary and Concluding Remarks

[57] EDUL peridotites display, in terms of mineral chemistry and modal proportions of cpx, moderate

to highly refractory compositions not consistent with the very slow spreading rate of the SWIR, the inferred thickness of the crust and the compositions of the spatially associated basalts.

[58] EDUL cpx are, in the whole, enriched in Na₂O relative to cpx from Atlantic peridotites for similar extents of melting. This enrichment in Na cannot be simply correlated with variable degrees of melting nor with metasomatic reactions in the subaxial lithospheric mantle.

[59] EDUL peridotites display strong heterogeneities and inconsistencies in modal and mineral compositions at scales ranging from the dredge to the whole studied region. Maximum heterogeneities and maximum enrichment in Na occur in the regions characterized by the more rugged and deepest axial valleys, and where basalts show very high Na_{8.0} and anomalous geochemical features.

[60] To explain these features, we propose that the peridotites have preserved relics of older events - partial melting and metasomatism - that created compositional heterogeneities in the protolith of the SWIR mantle. A late stage of partial melting in relation to the decompression beneath the SWIR has weakly depleted the mantle protolith. This very small extent of melting, predicted by the models, has preserved the initial mantle heterogeneities. But it may also be responsible for the introduction of new heterogeneities. The present peridotites which result from this multistage evolution have lost the geochemical and mineralogical correlations that are commonly observed in more extensively residual abyssal peridotites. This more than one stage melting evolution is also in good agreement with the compositions of the associated basalts [Meyzen *et al.*, 2003].

Acknowledgments

[61] We thank Captain Desson and the crew of the Marion Dufresne, as well as Bernard Ollivier and the IFRTP team, for their efficiency in collecting tons of samples from the Southwest Indian ridge. We thank Michael Toplis, Jean-Pierre Lorand and Eric Humler for stimulating discussions. This paper greatly benefited from constructive comments by Henry Dick, Kevin Johnson and Roberta Rudnick. This work was supported by a CNRS (groupe ad-hoc OCEANS) grant. This is Publication 1846 of the Institut de physique du globe de Paris.

References

- Baker, M. B., and E. M. Stolper, Determining the composition of high-pressure mantle melts using diamond aggregates, *Geochem. Cosmochem. Acta*, *58*, 2811–2827, 1994.
- Baker, M. B., M. M. Hirschmann, M. S. Ghiorso, and E. M. Stolper, Compositions of near-solidus peridotite melts from experiments and thermodynamic calculations, *Nature*, *375*, 308–311, 1995.
- Blundy, J. D., T. J. Falloon, B. J. Wood, and J. A. Dalton, Sodium partitioning between clinopyroxene and silicate melts, *J. Geophys. Res.*, *100*, 15,501–15,515, 1995.
- Bonatti, E., A. Peyve, P. Kepezhinskas, N. Kurentsova, M. Seyler, S. Skolotnev, and G. Udintsev, Upper mantle heterogeneity below the Mid-Atlantic Ridge, *J. Geophys. Res.*, *97*, 4461–4476, 1992.
- Bonatti, E., M. Seyler, and N. Sushevskaya, A cold suboceanic mantle belt at the Earth's equator, *Science*, *261*, 315–320, 1993.
- Bottinga, Y., and C. J. Allègre, Partial melting under spreading ridges, *Philos. Trans. R. Soc. London Ser. A*, *288*, 501–525, 1978.
- Bown, J. W., and R. S. White, Variation with spreading rate of oceanic crustal thickness and geochemistry, *Earth Planet. Sci. Lett.*, *121*, 435–449, 1994.
- Boyd, F. R., Compositional distinction between oceanic and cratonic lithosphere, *Earth Planet. Sci. Lett.*, *96*, 15–26, 1989.
- Cannat, M., and M. Seyler, Transform tectonics, metamorphic plagioclase and amphibolitization in ultramafic rocks of the Vema Transform Fault (Atlantic ocean), *Earth Planet. Sci. Lett.*, *133*, 283–298, 1995.
- Cannat, M., C. Rommevaux-Justin, D. Sauter, C. Deplus, and V. Mendel, Formation of the axial relief at the very slow spreading Southwest Indian Ridge (49° to 69°E), *J. Geophys. Res.*, *104*, 22,825–22,843, 1999.
- Debayle, E., and J. J. Lévêque, Upper mantle heterogeneities in the Indian ocean from waveform inversions, *Geophys. Res. Lett.*, *24*, 245–248, 1997.
- DeMets, C., R. G. Gordon, D. F. Argus, and C. Stein, Current plate motion, *Geophys. J. Int.*, *101*, 425–478, 1990.
- Dick, H. J. B., Abyssal peridotites, very slow spreading ridges and ocean ridge magmatism, in *Magmatism in the Ocean Basins*, edited by A. E. Saunders and M. J. Norris, pp. 71–105, Geol. Soc. Am., Boulder, Colo., 1989.
- Dick, H. J. B., R. L. Fisher, and W. B. Bryan, Mineralogic variability of the uppermost mantle along mid-ocean ridges, *Earth Planet. Sci. Lett.*, *69*, 88–106, 1984.
- Dupré, B., and C. J. Allègre, Pb-Sr isotope variation in Indian ocean basalts and mixing phenomena, *Nature*, *303*, 142–146, 1983.
- Falloon, T. J., and D. H. Green, Anhydrous partial melting of MORB pyroxene and other peridotite compositions at 10 kbar: Implications for the origin of primitive MORB glasses, *Mineral. Petrol.*, *37*, 181–219, 1987.
- Falloon, T. J., D. H. Green, H. S. O'Neill, and W. O. Hibberson, Experimental tests of low degree peridotite partial melt compositions: implications for the nature of anhydrous near-

- solidus peridotite melts at 1.0 GPa, *Earth Planet. Sci. Lett.*, **152**, 149–162, 1997.
- Falloon, T. J., D. H. Green, L. V. Danyushevsky, and U. H. Faul, Peridotite melting at 1.0 and 1.5 GPa: An experimental evaluation of techniques using diamond aggregates and mineral mixes for determination of near-solidus melts, *J. Petrol.*, **40**, 1343–1375, 1999.
- Forsyth, D. W., Geophysical constraints on mantle flow and melt generation beneath ocean-ridges, in *Mantle Flow and Melt Generation at Mid-Ocean Ridges*, *Geophys. Monogr. Ser.*, vol. 71, edited by J. Phipps-Morgan, pp. 1–66, AGU, Washington, D.C., 1992.
- Fox, P. J., and D. G. Gallo, A tectonic model for ridge-transform-ridge plate boundaries: Implications for the structure of oceanic lithosphere, *Tectonophysics*, **104**, 205–242, 1984.
- Francis, T. J. G., and R. W. Raitt, Seismic refraction measurements in the southern Indian ocean, *J. Geophys. Res.*, **72**, 3015–3041, 1967.
- Ghose, I., M. Cannat, and M. Seyler, Transform fault effect on mantle melting in the MARK area (Mid-Atlantic Ridge South of the Kane Transform), *Geology*, **24**, 1139–1142, 1996.
- Hart, S. R., A large-scale isotope anomaly in the Southern Hemisphere mantle, *Nature*, **309**, 753–757, 1984.
- Hart, S. R., and A. Zindler, In search of bulk Earth composition, *Chem. Geol.*, **57**, 247–267, 1986.
- Hellebrand, E., J. E. Snow, H. J. B. Dick, and A. W. Hofmann, Coupled major and trace-element melting indicators in mid-ocean ridge peridotites, *Nature*, **410**, 677–681, 2001.
- Hirose, K., and I. Kushiro, Partial melting of dry peridotites at high pressures: Determination of compositions of melts segregated from peridotite using aggregates of diamond, *Earth Planet. Sci. Lett.*, **114**, 477–489, 1993.
- Humler, E., C. Meyzen, J. Ludden, and C. Mével, Geochemical variations in basaltic glasses from the Southwest Indian Ridge (49 to 69°E), *Eos Trans. AGU*, **79**(45), F878, Fall Meet. Suppl., 1998.
- Jagoutz, E., H. Palme, H. Blum, M. Cendales, G. Dreibus, B. Spettel, V. Lorenz, and H. Wänke, The abundances of major, minor and trace elements in the earth's mantle as derived from primitive ultramafic nodules, in *Proceedings of the 10th Lunar and Planetary Science Conference*, *Geochim. Cosmochim. Acta*, **11**, 2031–2050, 1979.
- Johnson, K. T. M., and H. J. B. Dick, Open system melting and the temporal and spatial variation of peridotite and basalt compositions at the Atlantis II F.Z., *J. Geophys. Res.*, **97**, 9219–9241, 1992.
- Johnson, K. T. M., H. J. B. Dick, and N. Shimizu, Melting in the oceanic upper mantle: An ion microprobe study of diopsides in abyssal peridotites, *J. Geophys. Res.*, **95**, 2661–2678, 1990.
- Kelemen, P. B., G. Hirth, N. Shimizu, M. Spiegelman, and H. J. B. Dick, A review of melt migration processes in the adiabatically upwelling mantle beneath oceanic spreading ridges, *Philos. Trans. R. Soc. London*, **355**, 283–318, 1997.
- Kelemen, P. B., S. R. Hart, and S. Bernstein, Silica enrichment in the continental upper mantle via melt/rock reaction, *Earth Planet. Sci. Lett.*, **164**, 387–406, 1998.
- Kinzler, R. J., Melting of mantle peridotite at pressures approaching the spinel to garnet transition: Application to mid-ocean ridge basalt petrogenesis, *J. Geophys. Res.*, **102**, 853–874, 1997.
- Kinzler, R. J., and T. L. Grove, Primary magmas of mid-ocean ridge basalt, 1, Experiments and methods, *J. Geophys. Res.*, **97**, 6885–6906, 1992a.
- Kinzler, R. J., and T. L. Grove, Primary magmas of mid-ocean ridge basalts, 2, Applications, *J. Geophys. Res.*, **97**, 6907–6926, 1992b.
- Klein, E. M., and C. H. Langmuir, Global correlations of ocean ridge basalt chemistry with axial depth and crustal thickness, *J. Geophys. Res.*, **92**, 8089–8115, 1987.
- Komor, C., T. L. Grove, and R. Hébert, Abyssal peridotites from ODP hole 670A (21°10'N, 45°02'W): residues of mantle melting exposed by non-constructive axial divergence, *Proc. Ocean Drill. Program Sci. Results*, **106–109**, 85–101, 1990.
- Langmuir, C. H., E. M. Klein, and T. Planck, Petrological systematics of mid-ocean ridge basalts: Constraints on melt generation beneath ocean ridges, in *Mantle Flow and Melt Generation at Mid-Ocean Ridges*, *Geophys. Monogr. Ser.*, vol. 71, edited by J. Phipps-Morgan, pp. 183–280, AGU, Washington, D.C., 1992.
- Lundstrom, C. C., Rapid diffusive infiltration of sodium into partially molten peridotite, *Nature*, **403**, 527–530, 2000.
- McDonough, W. F., and S.-S. Sun, The composition of the Earth, *Chem. Geol.*, **120**, 223–253, 1995.
- McDonough, W. F., H. G. Stosch, and N. G. Ware, Distribution of titanium and the rare earth elements between peridotitic minerals, *Contrib. Mineral. Petrol.*, **110**, 321–328, 1992.
- McKenzie, D., and M. J. Bickle, The volume and composition of melt generated by extension of the lithosphere, *J. Petrol.*, **29**, 625–679, 1988.
- McKenzie, D., and R. K. O'Nions, The source regions of ocean island basalts, *J. Petrol.*, **36**, 1995.
- Mendel, V., D. Sauter, L. M. Parson, and J. R. Vanney, Segmentation and morphotectonic variations along an ultra-slow spreading center: The South West Indian Ridge (57°E–70°E), *Mar. Geophys. Res.*, **19**, 503–533, 1997.
- Mével, C., Sampling the Southwest Indian Ridge: First results of the EDUL cruise (R/V *Marion Dufresne II*, August 1997), *InterRidge News*, **6-2**, 25–26, 1997.
- Meyzen, C., E. Humler, J. Ludden, M. J. Toplis, and C. Mével, Unique MORB compositions from the Southwest Indian Ridge, paper presented at South West Indian Ridge Inter-Ridge Workshop, Southampton Oceanographic Centre, Southampton, U.K., 2002.
- Meyzen, C., E. Humler, J. Ludden, M. J. Toplis, and C. Mével, Geochemical indicators of a major discontinuity in mantle composition along with Southwest Indian Ridge, *Nature*, in press, 2003.
- Michael, P. J., and E. Bonatti, Peridotite composition from the North Atlantic: Regional and tectonic variations and implications for partial melting, *Earth Planet. Sci. Lett.*, **73**, 91–104, 1985.
- Muller, M. R., C. J. Robinson, T. A. Minshull, R. S. White, and M. J. Bickle, Thin crust beneath ocean drilling program

- borehole 735B at the Southwest Indian Ridge?, *Earth Planet. Sci. Lett.*, *148*, 93–107, 1997.
- Muller, M. R., T. A. Minshull, and R. S. White, Crustal structure and segmentation on the SWIR at 66°E (abstract), paper presented at European Geophysical Society Symposia, Nice, France, 1998.
- Niu, Y., Mantle melting and melt extraction processes beneath ocean ridges: Evidence from abyssal peridotites, *J. Petrol.*, *38*, 1047–1074, 1997.
- Patriat, P., and J. Segoufin, Reconstruction of the central Indian Ridge Ocean, *Tectonophysics*, *155*, 211–234, 1988.
- Patriat, P., D. Sauter, M. Munsch, and L. Parson, A survey of the Southwest Indian Ridge axis between Atlantis II FZ and the Indian Ocean Triple Junction: Regional setting and large-scale segmentation, *Mar. Geophys. Res.*, *19*, 457–480, 1997.
- Pickering-Witter, J. M., and A. D. Johnston, The effects of variable mineral proportions on the melting systematics of fertile peridotite assemblages, *Contrib. Mineral. Petrol.*, *140*, 190–211, 2000.
- Price, R. C., A. K. Kennedy, M. Riggs-Sneeringer, and F. A. Frey, Geochemistry of basalts from the Indian ocean ridge triple junction: Implications for the generation and evolution of Indian ocean ridge basalts, *Earth Planet. Sci. Lett.*, *78*, 379–396, 1986.
- Putirka, K., Melting depths and mantle heterogeneity beneath Hawaii and the East Pacific Rise: Constraints from Na/Ti and rare earth element ratios, *J. Geophys. Res.*, *104*, 2817–2829, 1999.
- Rampone, E., P. Bottazzi, and L. Ottolini, Complementary Ti and Zr anomalies in orthopyroxene and clinopyroxene from mantle peridotites, *Nature*, *354*, 518–521, 1991.
- Reid, I., and H. R. Jackson, Oceanic spreading rate and crustal thickness, *Mar. Geophys. Res.*, *5*, 165–172, 1981.
- Robinson, C. J., R. S. White, M. J. Bickle, and T. A. Minshull, Restricted melting under the very slow spreading Southwest Indian Ridge, in *Tectonic, Magmatic, Hydrothermal and Biological Segmentation of Mid-Ocean Ridges*, edited by C. J. McLeod et al., pp. 131–141, Geol. Soc. of Am., Boulder, Colo., 1996.
- Robinson, J. A. C., B. J. Wood, and J. D. Blundy, The beginning of melting of fertile and depleted peridotite at 1.5 GPa, *Earth Planet. Sci. Lett.*, *155*, 97–111, 1998.
- Schwab, B. E., and D. A. Johnston, Melting systematics of modally variable, compositionally intermediate peridotites and the effects of mineral fertility, *J. Petrol.*, *42*, 1789–1811, 2001.
- Seyler, M., and E. Bonatti, Na, Al^{IV} and Al^{VI} in clinopyroxenes of subcontinental and suboceanic ridge peridotites: A clue to different melting processes in the mantle?, *Earth Planet. Sci. Lett.*, *122*, 281–289, 1994.
- Seyler, M., and E. Bonatti, Regional-scale melt-rock interaction in Iherzolitic mantle in the Romanche Fracture Zone (Atlantic ocean), *Earth Planet. Sci. Lett.*, *146*, 273–287, 1997.
- Seyler, M., M. J. Toplis, J.-P. Lorand, A. Luguët, and M. Cannat, Clinopyroxene microtextures reveal incompletely extracted melts in abyssal peridotites, *Geology*, *29*, 155–158, 2001.
- Seyler, M., M. J. Toplis, J.-P. Lorand, G. Godard, and A. Luguët, Hydrous mineral inclusions in harzburgites from the Southwest Indian Ridge, paper presented at South West Indian Ridge InterRidge Workshop, Southampton Oceanographic Centre, Southampton, U.K., 2002.
- Shen, Y., and D. Forsyth, Geochemical constraints on initial and final depths of melting beneath mid-ocean ridges, *J. Geophys. Res.*, *100*, 2211–2237, 1995.
- Smith, W. H. F., and D. T. Sandwell, Bathymetry prediction from dense satellite altimetry and sparse shipboard bathymetry, *J. Geophys. Res.*, *99*, 21,803–21,824, 1994.
- Stephens, C. J., Heterogeneity of oceanic peridotite from the western canyon wall at MARK: results from site 920, *Proc. Ocean Drill. Program Sci. Results*, *153*, 285–301, 1997.
- Sun, S.-S., and W. F. McDonough, Chemical and isotopic systematics of oceanic basalts: implications for mantle composition and processes, in *Magmatism in the Ocean Basins*, edited by A. D. Saunders and M. J. Norry, pp. 313–345, Geol. Soc. of Am., Boulder, Colo., 1989.
- Walter, M. J., Comments on “Mantle Melting and Melt Extraction Processes beneath Ocean Ridges: Evidence from Abyssal Peridotites” by Yaoling Niu, *J. Petrol.*, *40*, 1187–1193, 1999.
- White, R. S., T. A. Minshull, M. J. Bickle, and C. J. Robinson, Melt generation at very slow-spreading oceanic ridges: Constraints from geochemical and geophysical data, *J. Petrol.*, *42*, 1171–1196, 2001.